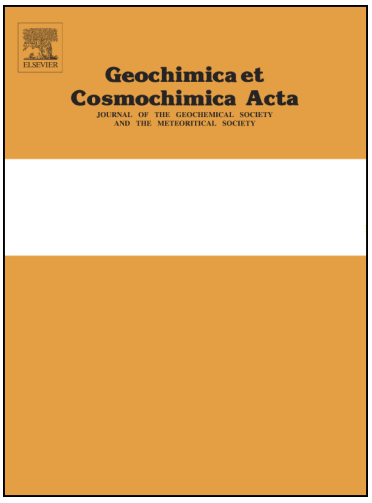

Rhenium-osmium isotopes and highly siderophile elements in ultramafic rocks from the Eoarchean Saglek Block, northern Labrador, Canada: implications for Archean mantle evolution

Akira Ishikawa, Katsuhiko Suzuki, Kenneth D. Collerson, Jingao Liu, D. Graham Pearson, Tsuyoshi Komiya

PII: S0016-7037(17)30447-7
DOI: http://dx.doi.org/10.1016/j.gca.2017.07.023
Reference: GCA 10385

To appear in: *Geochimica et Cosmochimica Acta*

Received Date: 20 December 2016
Revised Date: 7 July 2017
Accepted Date: 11 July 2017

Please cite this article as: Ishikawa, A., Suzuki, K., Collerson, K.D., Liu, J., Graham Pearson, D., Komiya, T., Rhenium-osmium isotopes and highly siderophile elements in ultramafic rocks from the Eoarchean Saglek Block, northern Labrador, Canada: implications for Archean mantle evolution, *Geochimica et Cosmochimica Acta* (2017), doi: http://dx.doi.org/10.1016/j.gca.2017.07.023

Rhenium-osmium isotopes and highly siderophile elements in ultramafic rocks from the Eoarchean Saglek Block, northern Labrador, Canada: implications for Archean mantle evolution

Akira Ishikawa[1,2]*, Katsuhiko Suzuki[2], Kenneth D. Collerson[3], Jingao Liu[4,5], D. Graham Pearson[4], Tsuyoshi Komiya[1]

[1]Department of Earth Science and Astronomy, Graduate School of Arts and Sciences, The University of Tokyo, Tokyo 153-8902, Japan

[2]Research and Development Center for Submarine Resources, Japan Agency for Marine Earth Science and Technology (JAMSTEC), Yokosuka 236-0016, Japan

[3]School of Earth and Environmental Sciences, University of Queensland, Brisbane, Qld 4072, Australia

[4]Department of Earth and Atmospheric Sciences, University of Alberta, Edmonton, T6G 2E3, Canada

[5]State Key Laboratory of Geological Processes and Mineral Resources, China University of Geosciences, Beijing 100083, China

*corresponding author: akr@ea.c.u-tokyo.ac.jp

phone: +81-3-5454-6364

fax: +81-3-5465-8244

To be submitted to: Geochimica et Cosmochimica Acta

Draft: 20th December 2016, **Revision:** 5th June 2017, **Re-revision:** 7th July 2017

Keywords: Highly siderophile element, Re-Os systematics, peridotite, komatiite, mantle, early Archean, late accretion

Word Count: 11096 main text + abstract

Figure Count: 9

Table Count: 4

ABSTRACT

We determined highly siderophile element (HSE: Os, Ir, Ru, Pt, Pd, and Re) concentrations and $^{187}Os/^{188}Os$ ratios for ultramafic rocks distributed over the Eoarchean gneiss complex of the Saglek-Hebron area in northern Labrador, Canada in order to constrain to what extent variations in HSE abundances are recorded in Early Archean mantle that have well-resolved ^{182}W isotope anomalies relative to the present-day mantle (~+11 ppm: Liu et al., 2016). The samples analysed here have been previously classified into two suites: mantle-derived peridotites occurring as tectonically-emplaced slivers of lithospheric mantle, and metakomatiites comprising mostly pyroxenitic layers in supracrustal units dominated by amphibolites. Although previous Sm-Nd and Pb-Pb isotope studies provided whole-rock isochrons indicative of ~3.8 Ga protolith formation for both suites, our whole-rock Re-Os isotope data on a similar set of samples yield considerably younger errorchrons with ages of 3612 ± 130 Ma (MSWD = 40) and 3096 ± 170 Ma (MSWD = 10.2) for the metakomatiite and lithospheric mantle suites, respectively. The respective initial $^{187}Os/^{188}Os$ = 0.10200 ± 18 for metakomatiites and 0.1041 ± 18 for lithospheric mantle rocks are within the range of chondrites. Re-depletion Os model ages for unradiogenic samples from the two suites are consistent with the respective Re-Os errorchrons (metakomatiite T_{RD} = 3.4-3.6 Ga; lithospheric mantle T_{RD} = 2.8-3.3 Ga). These observations suggest that the two ultramafic suites are not coeval. However, the estimated mantle sources for the two ultramafics suites are similar in terms of their broadly chondritic evolution of $^{187}Os/^{188}Os$ and their relative HSE patterns. In detail, both mantle sources show a small excess of Ru/Ir similar to that in modern primitive mantle, but a ~20% deficit in absolute HSE abundances relative to that in modern primitive mantle (metakomatiite 74 ± 18% of PUM; lithospheric mantle 82 ± 10% of PUM), consistent with the ~3.8 Ga Isua mantle source and Neoarchean komatiite sources around the world (~70-86% of PUM). This demonstrates that the lower HSE abundances are not unique to the sources of komatiites, but rather might be a ubiquitous feature of Archean convecting mantle. This tentatively suggests that chondritic late accretion components boosted the convecting mantle HSE inventory after core separation in the Hadean, and that the Eoarchean to Neoarchean convecting mantle was depleted in its HSE content relative to that of today. Further investigation of Archean mantle-derived rocks is required to explore this hypothesis.

1. Introduction

The overabundance of highly siderophile elements (HSEs: Re, Os, Ir, Ru, Pt, Rh, Pd, Au) in the modern terrestrial mantle, relative to its predicted composition based on the low-pressure metal-silicate partitioning data is frequently attributed to the late influx of chondritic materials after the efficient stripping of the HSEs to the metallic core (e.g. Kimura et al., 1974; Chou, 1978). This concept, known as late accretion or late veneer (hereafter the former term is mainly used), is not universally accepted due to insufficient knowledge of metal-silicate partitioning under high-pressure and temperature conditions. However, the broadly chondritic ratios of HSEs in modern terrestrial mantle deduced from a variety of mantle peridotites and chondritic Pt/Os and Re/Os required in present-day Os isotopes of mantle-derived rocks provide strong support for the late accretion over other competing hypotheses such as metal-silicate equilibrium at the base of a deep-magma ocean (e.g. Becker et al., 2006; Walker, 2009; Mann et al., 2012; Chatterjee and Lassiter, 2016; Day et al., 2017). Elevated HSE abundances in broadly chondritic proportions are also recognised in a wide-variety of achondrites, demonstrating that late accretion was a common feature of all differentiated planetary bodies (Day et al., 2007; Dale et al., 2012; Day et al., 2012; Riches et al., 2012; van Acken et al., 2012; Day and Walker, 2015). Since it is proposed that late accretion was a major control on both the amount the HSEs and Earth's volatile components, including water (e.g. Albarede, 2009), the nature of late accretion is an important issue for understanding the history of terrestrial planets and the Solar System.

A commonly held view of the Earth-Moon system is that the Moon-forming giant impact created the final global magma ocean, enhancing core-mantle differentiation in the two bodies, and was critical to defining the geochemistry of the late accretion era, initiated immediately following the final phase of core formation induced by the giant impact. Although there is no consensus on the age of the Moon, chronological data obtained from the oldest lunar crustal rocks, such as ferroan anorthosites considered to be primary floatation-cumulates of a lunar magma ocean, tend to provide relatively younger ages of around 4.4 Ga (e.g. Norman et al., 2003; Borg et al., 2011). By contrast, recent *N*-body simulations (Jacobson et al., 2014) demonstrate a relationship between the timing of giant impact and the amount of late accreted mass, suggesting that a Moon-formation age of 95 ± 32 Myr (after the beginning of Solar System) can account for the amount of late accreted mass (0.48 ± 0.16 % of the present Earth's mass), calculated using the observed Earth's mantle budget of HSEs and the average of chondrites (Becker et al., 2006; Walker, 2009). This estimated age is broadly consistent with the current constraints from the short-lived ^{182}Hf-^{182}W system, which is sensitive to early fractionation between lithophile Hf and

siderophile W during core formation, although late accretion provides very low resolution to the Hf-W chronometer as a time of Earth-Moon formation. The $^{182}W/^{184}W$ ratios of the modern terrestrial rocks are ~200 ppm more radiogenic than those in chondrites (Kleine et al., 2002; Schoenberg et al., 2002; Yin et al., 2002), whereas they are slightly unradiogenic (~20-30 ppm) relative to the lunar mantle (Kruijer et al., 2015; Touboul et al., 2015). These ^{182}W results can be explained by a model where terrestrial core formation was largely completed during the first ~60 Myr after the beginning of the Solar System, while the ^{182}Hf nuclide was still extant. Slightly later, the formation of the Moon led to the final phase of Earth's core separation, after ^{182}Hf was extinct. The ensuing late accretion then created the large difference in absolute HSE abundances together with the small ^{182}W difference observed between the mantle of Earth and the Moon, that are explained by disproportional late accretion to the two bodies (Day et al., 2007; Day and Walker, 2015; Kruijer et al., 2015; Touboul et al., 2015).

One of the major uncertainties related to late accretion on the Earth is the time frame of delivery of late accreted materials and subsequent homogenisation within the mantle. Based on the chondritic $^{187}Os/^{188}Os$ compositions of 3.81-Ga metaperidotites from southwest Greenland, Bennett et al. (2002) concluded that any HSE-rich late accretionary components must have been added to the Earth, incorporated into and grossly homogenised within the mantle by 3.8 Ga. Furthermore, these authors emphasised that the late accretion on the Earth does not coincide with the era known as the late heavy bombardment (~4.1-3.8 Ga) which created the late stage impact basins on the Moon (Tera et al., 1974). However, Willbold et al. (2011) discovered ~15 ppm enrichments in $^{182}W/^{184}W$ relative to modern terrestrial mantle in ~3.8 Ga crustal rocks from the Isua supracrustal belt in southwest Greenland, and claimed that this area of Earth's surface escaped the addition of a chondritic late accretionary component. Similar magnitudes of ^{182}W anomaly are now recognised in other Eoarchean terrains such as the Nuvvuagittuq greenstone belt in northern Quebec, Canada (Touboul et al., 2014), the Acasta gneiss complex in Northwest Territories, Canada (Willbold et al., 2015) and Saglek Block in northern Labrador, Canada (Liu et al., 2016), suggesting that a globally constant signature of the Hadean mantle existed prior to the late accretionary processes and is uniformly recorded in Eoarchean rocks (Willbold et al., 2015; Dale et al., 2017). This scenario implies a significant contribution of the late heavy bombardment component to the present-day mantle, or that mixing of an earlier veneer into Earth's mantle was slow, incomplete or initially delayed, contrary to the previous assertions (Bennett et al., 2002).

Studies using komatiitic lavas of various ages as mantle probes indicate a possible secular increase of HSE abundances in their mantle sources from ~3.5 to ~2.9 Ga, which can be attributed to progressive pollution by the late accretionary component down into the HSE-poor deeper mantle in the period between the late heavy bombardment and Neoarchean (Maier et al., 2009; Fiorentini, 2011). This hypothesis seems apparently consistent with the notion that the elevated ^{182}W signature in Eoarchean rocks reflect a deficiency in late accretionary components. However, combined ^{182}W and HSE data for ~2.9 Ga Kostomuksha komatiites (Baltic shield, Russia) and ~3.48 Ga Komati komatiites (Barberton greenstone belt, South Africa) cast doubt on the late accretion origin of ^{182}W enrichments because the younger, HSE-poor Kostomuksha source exhibits a ^{182}W excess of ~15 ppm, while older, HSE-poor Komati source has no resolvable excess (Touboul et al., 2012). More recently, a negative ^{182}W anomaly has been reported for one of the oldest ~3.55 Ga Schapenburg komatiites (Barberton greenstone belt, South Africa) characterised by the lowest known HSE abundances in their mantle source, compared to other early Archean komatiites (Puchtel et al., 2016a). This combination of low HSE abundances and ^{182}W deficit is clearly inconsistent with a late accretion origin for the ^{182}W variation, while the ^{142}Nd deficit coupled with these anomalies led Puchtel et al. (2016a) to conclude that they were likely produced by an early mantle differentiation event. It seems now generally agreed that such early-formed ^{182}W heterogeneities have survived to the present-day in the Earth's deep interior from recent discoveries of ^{182}W enrichment in Mesozoic and younger Baffin Island picrites and Ontong Java Plateau basalts (Rizo et al., 2016a), as well as the ^{182}W depletion in high-^{3}He basalts from Hawaii and Samoa (Mundl et al., 2017). Overall, the origin of ^{182}W anomalies in terrestrial samples including the uniform ^{182}W-enriched signature recorded in Eoarchean rocks remains uncertain. Thus, understanding to what extent variations in HSE abundances are recorded in Eoarchean mantle is crucial for deciphering its evolution to the present-day mantle via late accretion and subsequent homogenisation.

Here we examine HSE abundances and ^{187}Re-^{187}Os isotopic systematics for a set of ultramafic rocks from the extensive gneiss complex of the Saglek-Hebron area in northern Labrador, located on the western margin of the North Atlantic Craton. In this region, Collerson et al. (1991) identified two suites of ultramafic rocks from the Eoarchean supracrustal unit, based on field occurrences and geochemical data. A group of metamorphosed peridotites were regarded as tectonically-emplaced slivers of residual mantle (the lithospheric mantle suite). Another group was identified as a sequence of metamorphosed komatiites in the supracrustal units (the metakomatiite suite). Both

lithospheric mantle and metakomatiite suites yield statistically identical linear arrays on a whole-rock ^{147}Sm-^{143}Nd isochron with slopes equivalent to 3815 ± 121 Ma and 4017 ± 194 Ma, respectively (Collerson et al., 1991). Although these ultramafic rocks underwent high-grade metamorphism at ~2.7-2.8 Ga significantly after their emplacement, a consistent Pb-Pb errorchron of 3845 ± 160 Ma was obtained from whole rock analysis of the metakomatiite suite, supporting their ~3.8 Ga formation (Wendt and Collerson, 1999) and indicating minimal chemical disturbance. More recently, Liu et al. (2016) have identified well-resolved positive ^{182}W anomalies (~11 ± 3 ppm) for many of mafic-ultramafic rocks investigated here, and Morino et al. (2017) reported a virtually identical but more precise ^{147}Sm-^{143}Nd age of 3782 ± 92 Ma for mafic-ultramafics rocks hosting positive ^{142}Nd anomalies (8.6 ± 3.3 ppm). Considering that Re-Os isotope and HSE systematics should be much less susceptible to contamination of crustal components than W, Nd and Pb isotopes, these ultramafic rocks preserving short-lived ^{142}Nd and ^{182}W isotope anomalies are suitable samples for constraining the HSE abundances of mantle source in Eoarchean and the processes involved in their generation.

2. Geological, geochronological background and sample details

The Saglek-Hebron area is located in the northeastern coast of Labrador Peninsula, Canada, and forms the western margin of North Atlantic Craton extending from Scotland through Greenland to Labrador (Fig. 1: Bridgwater and Schiøtte, 1991). This area is dominated by Early and Late Archean suites of tonalitic, trondhjemitic and granodioritic gneisses (TTG) and a heterogeneous group of supracrustal units, both of which underwent high-grade granulite to amphibolite facies metamorphism at 2.7 to 2.8 Ga. The area is separated into two parts by a major, NS-trending, sub-vertical fault, termed the Handy fault. The western area is characterised by the granulite facies mineral assemblages, and the eastern domain is dominated by amphibolite facies gneisses. Both the western and eastern parts, are cut by younger granite intrusions with ages of ca. 2.5 Ga and by EW trending Proterozoic mafic dykes.

Based on the geological setting and some chronological constraints, the orthogneisses in the Saglek-Hebron area can be classified into two groups (Bridgewater et al., 1975; Hurst et al., 1975): volumetrically important pre-3.5 Ga Uivak gneisses and a less dominant Lister gneiss dated at about 3.2 Ga (Schiøtte et al., 1989a). They can be distinguished in the field by the presence or absence of distinctive metamorphosed mafic dykes - the Saglek dykes (Collerson et al., 1982; Collerson et al., 1984), analogous to the criterion established for the Itsaq gneiss complex using the occurrence of Ameralik dykes (McGregor, 1973). It

has been proposed that the pre-3.5 Ga Uivak gneisses, older than Saglek dykes, are further subdivided into two suites: an early Uivak I gneiss with TTG compositions, extensively distributed in the area; and a younger suite of iron-rich porphyritic Uivak II gneiss, which can be shown occasionally in the field to have intruded into the earlier Uivak I gneiss (Bridgewater and Collerson, 1976). Based on the zircon U-Pb chronology, the protolith formation in the Uivak II gneisses has been estimated at ca. 3.62 Ga, whereas the protolith age of the Uivak I gneisses is the source of major debate, ranging from 3.73 Ga (Schiøtte et al., 1989a) to >3.95 Ga (Komiya et al., 2015; Shimojo et al., 2016).

The supracrustal units distributed over the Saglek/Hebron area can also be divided into two groups based on their cross-cutting relationships with the Saglek dykes: the pre-Saglek Nulliak; and post-Saglek Upernavik supracrustal groups. Both supracrustal groups are dominated by mafic and ultramafic rocks with subordinate chemical and clastic sedimentary rocks. Since the distinguishing criterion based on the presence or absence of Saglek dyke is ambiguous due to the common occurrence of amphibolite in both supracrustal units, the relative difference in lithological assemblages of sedimentary rocks are also considered to be useful for separating the two units: the presence of banded iron formation (BIF) is restricted to the older Nulliak supracrustal units, whereas pelitic rocks are regarded as the representative sedimentary rocks in the younger Upernavik supracrustal units (Ryan and Martineau, 2012).

As with the case of Uivak gneisses, the ages of Nulliak supracrustal rocks remain controversial because they rely heavily on the ages and field occurrences of associated orthogneisses. In most places, the boundaries between the Nulliak supracrustal units and the Uivak orthogneisses are equivocal largely because of later intense deformation. However, judging from the primary intrusive contacts preserved in some places, it is considered that the Nulliak supracrustal rocks are older than the Uivak gneisses (Komiya et al., 2015; Shimojo et al., 2016). Using radiometric dating, several efforts have been made to determine the magmatic crystallization or depositional ages of the Nulliak supracrustal rocks. Schiøtte et al. (1989b) reported a SHRIMP U-Pb age of 3776 ± 8 Ma for igneous zircons extracted from a garnet-biotite gneiss, and interpreted the age as the deposition of an acid-metavolcanic rock in the Nulliak supracrustal unit. A similar age was recorded in some of detrital zircons extracted from a Nulliak assemblage quartzite (ca. 3800 Ma), which also contained older grains, up to 3845 ± 50 Ma (Nutman and Collerson, 1991).

The magmatic crystallization ages of predominant mafic and ultramafic rocks in Nulliak supracrustal units are largely undetermined because of widespread effects of late Archean high-grade metamorphism. However, one ultramafic rock suite exposed in the vicinity of

Jerusalem Harbour near Hebron (Fig. 1) shows good agreement between ^{147}Sm-^{143}Nd and Pb-Pb whole rock errorchrons of 4017 ± 194 Ma and 3845 ± 160 Ma, respectively, and is considered to represent a sequence of metakomatiites generated via melting of the early Archean mantle (Collerson et al., 1991; Wendt and Collerson, 1999). The Eoarchean age of this unit has recently been confirmed by the study of ^{146}Sm-^{142}Nd and ^{147}Sm-^{143}Nd for mafic-ultramafic samples newly collected in same location (Fig. 1), which yields a more precise ^{147}Sm-^{143}Nd age of 3782 ± 93 Ma (Morino et al., 2017). Samples analysed in this study include five metakomatiites (KC87-111E, F, G, I and K) comprising mostly pyroxene-hornblende layers with subordinate amounts of olivine, and a metakomatiitic basalt (KC87-115D) dominated by hornblende coexisting with anorthitic plagioclase. The mineral assemblages of each sample is summarised in Table 1 and thin section photographs of representative sample (KC87-111F) are shown in Fig. 2. Although details of the specimens including mineral mode, whole rock major and trace element data were previously reported in Collerson et al. (1991), we performed petrographic and geochemical characterisation on newly prepared portions of the same specimens. It should be noted that clinopyroxene is totally absent in our studied portions of metakomatiites, and they are classified into olivine-pyroxene hornblendite (KC87-111F and G), olivine hornblendite (KC87-111I and K) and pyroxene hornblendite (KC87-111E) based on the IUGC nomenclature proposed by Streckeisen (1976).

Another ultramafic rock suite, interpreted as slivers of tectonically interleaved lithospheric mantle, is comprised of metaperidotites and metapyroxenites (hornblendites). They typically occur as blocks and enclaves within orthogneisses, and range in size from less-than 1 m elliptic bodies to a ~300 m-thick layered body forming outcrops that can be traced up to a few km along strike. The margins to the ultramafic outcrops, abutting the surrounding granitic rocks consist of a reaction zone of phlogopitic mica and serpentine. However, most bodies preserve fresh interiors dominated by olivine and pargasitic amphibole with subordinate amounts of chromite and orthopyroxene. Except for several larger bodies, they are predominantly coherent dunite and amphibole harzburgites (Table 1), characterised by a limited abundance of pyroxenes due to amphibole replacement. No modal layering is evident, defined by variations of olivine and pyroxene/amphibole ratios. Although primary contacts against mafic lithologies are not preserved in the units studied here because most of them are structurally transposed and highly interleaved, a rare gabbro-websterite-harzburgite-dunite sequence found on the western coast of Shuldham Island appears to be primary and quite different from the typical layered succession of komatiite flows (Arndt et al., 2008; Komiya et al., 2015). Thus, we consider that these

rocks are unlikely to be remnants of olivine-rich cumulate sequences in komatiite lava flows.

Collerson et al. (1991) examined samples of these ultramafic rocks collected from the vicinity of Iterungnek Fiord, which yield a whole rock Sm-Nd errorchron age of 3815 ± 121 Ma. However, Pb isotopic data for same sample suite display a poorly correlated array on Pb-Pb isochron diagram with an age of 2907 ± 560 Ma, which appears to record a contrasting evolution to that of metakomatiite suite (Wendt and Collerson, 1999). Recently, Morino et al. (2017) identified that a group of mafic-ultramafic rocks, without resolvable ^{142}Nd anomalies, yields a whole-rock ^{147}Sm-^{143}Nd isochron age of 3362 ± 100 Ma (MSWD = 4.5), and tentatively suggested their association with the Mesoarchean Upernavik supracrustal units. Although the geological significance of these ages is difficult to interpret, one of our aims is to test whether Re-Os systematics, presumably more robust to resetting and mixing with crustal components than Sm-Nd and Pb-Pb systematics, provide different age constraints. Hence, we selected samples that have been previously investigated for ^{147}Sm-^{143}Nd (KC87-102, KC87-106A, KC-87-114G and KC87-119A) and Pb-Pb systematics (KC87-104E, KC87-106A, KC87-114G, KC87-114I and KC87-114K). In addition to these seven samples and KC87-104D, we analysed samples from Big Island (KC91-52A, B, C and D), the eastern coast of St. John's Harbour (KC91-21A and B) and Cape Uivak (KC91-32A, B, C, D, E and F). Samples with the same number but different letter suffixes come from the same unit within an area of 20 x 30 m. The locations for each sample are shown in Fig. 1, and thin section photographs of representative samples are shown in Fig. 2. The ultramafic body located in the Cape Uivak is the largest of numerous exposed in the area, and is characterised by compositional layering on scales of centimetres to meters. The layering is comprised of amphibole harzburgite, olivine hornblendite and hornblendite. Although it is uncertain whether this body was emplaced as magmatic intrusion or tectonic inclusion, we treated the samples from this body separately from other members of the lithospheric mantle suite.

3. Analytical methods

All samples were sawn and their surfaces were ground off using carborundum to remove metal contaminants and weathered portions. Approximately, 50 g of each slab samples (thickness <1 cm) were disaggregated with a rock hammer by wrapping in plastic sheeting, washed in deionised water, dried, and then powdered in an alumina rod mill and an agate mortar/pestle. Whole rock major element concentrations were determined by X-ray fluorescence (XRF) on fused glass beads at Leicester University, UK. Trace element

analyses of selected samples were performed at the University of Alberta, Canada, using a *ThemoElement XR* inductively coupled plasma mass spectrometer (ICP-MS) via solution after HF-HNO_3 digestion of powder aliquots. Major and trace element concentrations measured for reference materials are presented in Table 1 and 2, respectively, along with their recommended values. Analytical precision and accuracy was typically better than 5 % for high-concentration elements (>0.5% for XRF, >1 ppm for ICP-MS), and better than 20 % for remaining low-concentrations elements. However, based on significant biases observed on some data for reference materials JP-1 and DTS-1, much greater uncertainties (<100 %) are realistic for very depleted elements. Forsterite contents in olivine [Fo = molar 100 Mg/(Mg+Fe)], spinel Mg- and Cr-number (Mg# = molar 100 $Mg/(Mg+Fe^{2+})$; Cr# = molar 100 Cr/(Cr+Al) were determined by electron probe micro-analyser (EPMA: JEOL-JXA8800) on thin sections at the University of Tokyo at Komaba, Japan. All analyses were performed with an accelerating voltage of 15 kV, 12 nA beam current and a counting time of 10-40 s. The oxide ZAF correction method was applied. For spinels, stoichiometric calculation for Fe^{3+} was applied.

Highly siderophile element (HSE) concentrations and Os isotope measurements were performed using isotope dilution (ID) mass spectrometry after Carius tube digestion (Shirey and Walker, 1995). The method used for sample digestion, chemical purification and mass spectrometry were based upon procedures outlined by Ishikawa et al. (2014). Approximately 1 g of powdered sample and spike solutions enriched in ^{185}Re and a mixed ^{190}Os-^{191}Ir-^{99}Ru-^{196}Pt-^{105}Pd were transferred into a Carius tube. After adding 10 ml of the inverse aqua regia, each Carius tube was frozen in a mixture of ethanol and dry ice, sealed with an oxygen-propane torch, and then placed in an oven at 240˚C for at least 72 h. Desilicification procedures were not applied because extraction of HSEs from ultramafic rocks is largely independent of the use of HF (cf. Ishikawa et al., 2014; Luguet et al., 2015; Day et al., 2016b).

Isotopic measurements of the HSE were conducted using two types of mass spectrometer. Osmium concentrations and isotopic compositions were measured by negative thermal ionisation mass spectrometry (N-TIMS, Thermo Electron Triton) at JAMSTEC, Japan. Purified Os after CCl_4 solvent extraction (Cohen and Waters, 1996) and microdistillation (Birck et al., 1997) was loaded in HBr on baked 99.997% Alfa Aesar Pt wire and covered with a NaOH-$Ba(OH)_2$ activator solution. Analyses of the international Os isotope mass spectrometry standard DROsS (load size 0.2-0.4 ng) yields ^{187}Os/^{188}Os of 0.16091 ± 3 [2 standard error (SE), n=46) and 0.16098 ± 5 (2SE, n=49) by SEM jumping and Faraday cup static modes (10^{11} ohm resistors), respectively, which are in good

agreement with other laboratories (0.160924 ± 4 for 10-100 ng; Luguet et al., 2008; 0.160938 ± 22 for 1-3 ng; Liu and Pearson, 2014).

The average total procedural Os blank was 11.3 ± 6.2 pg (n=14, 1SD) with a $^{187}Os/^{188}Os$ ratio of 0.179 ± 0.013. Slightly elevated and variable Os blanks during the course of the analyses was caused by contamination of airborne volatile Os from a neighbouring laboratory (cf. Ishikawa et al., 2014; Senda and Ishikawa, 2014). After employing closed vaporisation devices for the evaporation of HBr containing sample Os, the average total procedural Os blank was significantly reduced to 0.8 ± 0.3 pg (n=9, 1SD). Thus, blank corrections were applied for all the analyses, which relates to each batch of digestion rather than a long-term average, and uncertainties of $^{187}Re/^{188}Os$ and $^{187}Os/^{188}Os$ were estimated by error propagation of blank uncertainties (typically 10~30%). However, blank contributions for the measured Os concentrations and $^{187}Os/^{188}Os$ ratios were mostly insignificant: less than 2.0% and 1.5%, respectively. The highest blank contributions for a sample with the lowest Os (~30 ppt in KC91-32C-4) were 32% for concentration and 6% for $^{187}Os/^{188}Os$ ratio.

All the other HSE were measured by the Q-pole type ICP-MS (Agilent 7500s) housed in the University of Tokyo at Komaba, whose sensitivity was enhanced by using a second expansion pump and a shield torch system. Sample and standard solutions were interspersed throughout the analytical sessions to monitor and correct for instrumental fractionation. The monitored masses of analytes and interferences are ^{89}Y, ^{90}Zr, ^{95}Mo, ^{97}Mo, ^{99}Ru, ^{100}Ru, ^{101}Ru, ^{105}Pd, ^{106}Pd, ^{108}Pd, ^{111}Cd ^{178}Hf, ^{185}Re, ^{187}Re, ^{191}Ir, ^{193}Ir, ^{194}Pt, ^{195}Pt, ^{196}Pt, and ^{202}Hg. Although all raw signal intensities of samples were corrected for the measured isobaric-oxide interferences, contributions of interferences to analyte signals are insignificant (<0.1%). The total procedural blanks for the analysed elements averaged are 1.4 ± 1.5 pg Ir, 5.1 ± 3.9 pg Ru, 194 ± 50 pg Pt, 23 ± 12 pg Pd and 0.4 ± 0.2 pg Re (n=14, 1SD). As with the Os, all analyses were blank corrected. It should be noted that blank contributions of Ir and Ru are negligible for all samples (<1 % and <3%, respectively), whereas contributions to Pt, Pd and Re were significant for some samples up to 79% (KC87-102 and 104D), 16% (KC87-104D and 104E) and 21% (KC87-111K), respectively.

The accuracy of our analytical methods was evaluated by measuring ultramafic reference materials such as UB-N and JP-1. Concentrations, as well as reproducibilities, have previously been reported in Ishikawa et al. (2014) and the data are presented in Table 4. Five replicates analyses performed on sample KC87-119A display good reproducibilities (3.3% RSD for $^{187}Os/^{188}Os$, 7.4% Os, 4.3% Ir, 4.1% Ru, 11% Pt, 5.1% Pd and 5.8% Re, n=5) compared to those for UB-N. Larger variabilities in HSE concentrations

are occasionally found in other duplicated samples (lithospheric mantle suite: KC91-21B, KC91-52B, KC91-52C, KC87-114K, KC87-102; metakomatiite suite: KC87-111E, KC88-111F, KC87-111G, KC87-111I, KC87-111K). Sample KC87-114K shows the largest variability in most elements (38% Os, 31% Ir, 6.5% Ru, 69% Pt, 23% Pd and 12% Re RSDs, n=2), but slightly better reproducibility for $^{187}Os/^{188}Os$ (0.8%) and some HSE ratios (7.8% for Os/Ir and 43% Pt/Ir) suggests a contribution of powder heterogeneity (nugget effect), rather than an analytical issue with concentration measurements. The heterogeneous distribution of HSEs in studied rocks is also illustrated from the data of KC87-119A2, which was obtained from a newly prepared powder of KC87-119A. The $^{187}Os/^{188}Os$ ratio and, Ir, Ru and Pd concentrations of this aliquot are outside the range of five replicates of KC87-119A. However, the observed magnitude of variations does not affect our main conclusions.

4. Results

4.1. Major and trace element compositions

Mineral assemblages and constituent olivine/spinel major element compositions are summarised in Table 1, whereas whole-rock major and trace element compositions are provided in Table 2 and 3, respectively. As demonstrated by previous studies, the mineral abundances and chemistry of Early Archean ultramafics have been variably influenced by high-grade metamorphism and surficial alteration, making it difficult to constrain their protoliths (e.g., Rollinson, 2007). The effects of metamorphism and secondary alteration on the Saglek ultramafics are well documented by the development of textually equilibrated amphibole-phlogopite and serpentine replacing olivine. In order to test to what extent the HSE geochemistry is resistant to these effects, we analysed a range of ultramafic rocks including highly altered samples - defined by lack of fresh olivine - selected from the lithological spectrum. For the lithospheric mantle suite, highly altered dunites (KC87-104D and KC91-52A) and olivine hornblendites (KC87-102 and KC87-114G) can be distinguished by higher loss on ignition values (LOI: 9-16 wt.%). The same is true in the metakomatiite suite, where a highly altered sample (KC87-111I) is characterised by a higher LOI value of 7.8 wt.% than other metakomatiite samples.

Olivine Fo content in peridotites is often considered to be a robust indicator for discriminating between residual mantle and mantle melts. This criterion, to a first order, can be used in distinguishing the lithospheric mantle and metakomatiite suites in the Saglek ultramafics: the lithospheric mantle suite tends to include high-Fo olivine,

consistent with the interpretation of Collerson et al. (1991) of a residual mantle origin. However, dunite KC91-21A and amphibole harzburgite KC87-119A are comprised of olivine with Fo~87, overlapping the range observed in the metakomatiite suite (Fo~82-88). The robustness of olivine Fo to secondary effects is questioned by the common presence of extremely high-Fo olivine (Fo~96-97) in amphibole-rich harzburgites from the Cape Uivak layered body, that are complementary to the very low Mg# in coexisting spinel ranging from 1.4 to 6.8. These unusual olivine-spinel compositions are unlikely to be primary, and probably result from later metamorphic reequilibration involving olivine-spinel Mg-Fe exchange reaction (Rollinson, 2007; Szilas et al., 2015).

Modally abundant Al- and Mg-poor spinels in amphibole-rich harzburgites from the Cape Uivak layered body (Fig. 2E) are highly oxidised, as demonstrated by their very high-Fe_2O_3 contents (54-66 wt.%), implying complete transformation of Cr-spinel into ferrit-chromite. Spinel Mg# in the lithospheric mantle suite shows broad anti-correlations with Cr# and Fe_2O_3 contents, indicating variable degrees of replacement of Cr-spinel by ferrit-chromite. Thus, these spinel compositions may have no bearing upon the magmatic history of these rocks, but rather record the prograde reaction between primary Cr-spinel and magnetite formed by prior serpentinisation, mainly under amphibolite-facies conditions. However, the metakomatiites tend to contain spinel with slightly lower Mg#, at a given Cr# than those in the lithospheric mantle suite, consistent with their inferred protoliths being mantle melts.

Despite the strong influence of metamorphism on mineral chemistry, some elemental concentrations in the whole rocks are considered to be affected relatively little either by metamorphism or by secondary alteration. As previously reported by Collerson et al. (1991), the lithospheric mantle and metakomatiite suites can be discriminated by their Mg/Si and Al/Si ratios, and plot within or close to the fields for modern oceanic peridotites and Archean komatiites, respectively (Fig. 3A). Dunites and amphibole harzburgites in the lithospheric mantle suite (including Cape Uivak samples) have higher Mg/Si (1.26-1.57) and lower Al/Si (0-0.07), whereas metakomatiites have lower Mg/Si (0.50-1.03) and higher Al/Si (0.11-0.28) than the values of primitive mantle estimates. However, olivine hornblendites and hornblendites in the lithospheric mantle suite (KC91-102, KC91-52C, KC87-106A and KC91-32C) are almost identical with metakomatiites in terms of observed ranges of Mg/Si and Al/Si ratios (0.54-1.08 and 0.11-0.22). It should be noted that the whole rock data set of Archean komatiites plotted in Fig. 3 includes both spinifex-textured lava flows and olivine-rich cumulate units from Al-depleted, Al-undepleted and Al-enriched komatiite types (e.g., Robin-Popieul et al., 2012), but is restricted to those found

in extrusive komatiite flow fields. The data from thick komatiitic dunite bodies of intrusive origin plot above and to the left of the field of Archean komatiites but overlap the field of oceanic peridotites because they are dominated by olivine adcumulates containing less than 1 wt% Al_2O_3 (e.g., Fiorentini et al., 2007).

Several elements show broad correlations against Mg/Si ratios or MgO (anhydrous basis) in all samples, which can be attributed to primary magmatic differentiation (Fig. 3B and C). Negative correlations are commonly observed for incompatible elements apart from highly mobile elements such as alkalis (Na, K, Rb and Cs), P, Sr, Ba, and light rare earth elements (LREE: La, Ce, Pr and Nd). In contrast, Ni and Co contents displays positive correlations because they behave as compatible elements during typical mantle melting and magma evolution. In contrast with Ni and Co, Cr contents do not define a clear trend against MgO (Fig. 3D). When viewed separately by rock suites and types, the Cr concentration data of high-MgO samples (>40 wt.%) such as dunites and amphibole harzburgites in the lithospheric mantle suite plot within the field of modern peridotites. However, Cr_2O_3 in amphibole harzburgites and olivine hornblendites from the Cape Uivak layered body is distinctively high, ranging from 0.56 to 2.3 wt.%, compared with other members of the lithospheric mantle suite (Cr_2O_3 <0.56 wt.%). This high Cr concentrations may be due to the enrichment of spinel in the protoliths of the layered body, possibly indicating original podiform chromite mineralisation. Metakomatiites, olivine hornblendites and hornblendites in the lithospheric mantle suite (KC91-102, KC91-52C, KC87-116A and KC87-106A) have 19.6-36.8 wt.% MgO and 0.26-0.6 wt.% Cr_2O_3, within the range of Archean komatiites.

Geochemical discrimination between metakomatiites and pyroxenitic members of the lithospheric mantle suite (olivine hornblendites and hornblendites) can only be made by their contrasting REE patterns (Fig. 4). The metakomatiites, excepting a low-Mg basaltic sample (KC87-115D), are depleted in LREEs relative to heavy REEs (HREEs: Tb, Dy, Ho, Er, Tm, Yb and Lu) with chondrite-normalised ratios of Ce_N/Yb_N = 0.38-0.53 and Nd_N/Yb_N = 0.32-0.51, showing some affinities with typical Al-enriched type of peridotitic komatiites (e.g., Robin-Popieul et al., 2012). Distinct from these signatures, all members of the lithospheric mantle suite tend to show flat to LREE-enriched chondrite-normalised patterns with Ce_N/Yb_N = 0.94-3.0 and Nd_N/Yb_N = 0.95-2.4, with most exhibiting negative Eu anomalies. The Mesoarchean suite studied by Morino et al. (2017) also displays relative LREE enrichment rather than the LREE depletion that dominates the Eoarchean suite, and strongly resembles the REE patterns of the amphibole-rich variant of the lithospheric mantle suite (Fig. 4B and D). As noted previously, Collerson et al. (1991) concluded that

neither the LREE enrichments nor Eu anomalies observed for both ultramafic suites have been related to ~2.7-2.8 Ga amphibolite-grade metamorphism or extent of surficial alteration based on their Eoarchean Sm-Nd ages. However, this is not the case for Pb and W isotope systematics because there are strong positive W, U and Pb anomalies in the incompatible trace element abundances for both suites (Fig. 4C and D). Since the protoliths of both ultramafic suites are expected to be very low in these incompatible elements, it is possible that the Pb and W isotopic signatures of their mantle sources can be overprinted at much later times (Wendt and Collerson, 1999; Liu et al., 2016).

4.2. Highly siderophile element abundances

Whole-rock HSE abundances for the Saglek ultramafics are presented in Table 3 and their CI chondrite-normalised patterns are plotted in Fig. 5. For replicated samples, the averaged values for each sample are plotted on the diagram. As is the case of major and trace elements, different lithological suites and types show distinct HSE patterns.

Despite the variable degrees of serpentinisation, dunites in the lithospheric mantle suite show coherent HSE patterns characterised by a broadly chondritic proportion of the Ir group platinum-group elements (IPGE: Os, Ir, Ru), and strong depletion in the Pt group PGE (PPGE: Pt, Pd), as well as Re (Fig. 5A). These PPGE depleted patterns are very similar to those in highly depleted harzburgite and dunite in cratonic xenoliths (e.g., Pearson et al., 2004; Aulbach et al., 2015), and plot within the range observed in less modified peridotite xenoliths from southwest Greenland in North Atlantic Craton, which preserve Archean Re-depletion Os model ages (Wittig et al., 2010). Similar PPGE-depleted HSE patterns were reported for pure olivine separates from olivine-cumulate units of the 3.3 Ga Weltevreden komatiites (Connolly et al., 2011; Puchtel et al., 2014). However, a much larger range of HSE variations than those seen in the olivine separates and cratonic dunite-harzburgites are typically observed in whole rock data for olivine cumulates (cf. Fig.4 of Puchtel et al., 2014). For example, Ir abundances and Pd_N/Ir_N in those showing essentially identical MgO contents in the 3.3 Ga Weltevreden komatiites vary from 1.0 to 11.0 ppb, and from 0.2 to 2.5, respectively, reflecting Os-Ir alloy saturation during komatiite lava differentiation (Puchtel et al., 2004; Barnes and Fiorentini, 2008). In contrast, despite their widespread occurrence, the dunites studied here possess a relatively limited range of Ir abundances (2.0-3.8 ppb) over a large range of MgO contents (43-50 wt.% recalculated to anhydrous), that is somewhat inconsistent with their cumulate origin but in line with an origin as residues from partial melting.

Amphibole-rich lithologies of the lithospheric mantle suite tend to have slightly lower IPGE and higher PPGE abundances (e.g., higher Ru/Pt ratios) than those in the dunites (Fig. 5B). Re abundances of these rocks are somewhat variable. Three out of seven samples are more enriched in Re than that in dunites, whereas the other shows strong depletion in Re. Overall, the amphibole-rich ultramafics in the lithospheric mantle suite show irregular patterns, which tend to deviate from the range observed in modern lithospheric mantle (e.g., Becker et al., 2006). It should be noted that some of ultramafic rocks from Isua supracrustal belts studied by Rizo et al. (2016b) display similar HSE patterns to our studied samples (Fig. 5B), but significantly different from those suggested to be igneous cumulates showing very high Pd_N/Ir_N (>10; Szilas et al., 2015). More recently, from the orthogneiss terrain adjacent to supracrustal belts in the Isua terrane, Dale et al. (2017) identified ultramafic samples having broadly chondritic relative HSE abundances, with absolute concentrations that fall at the lowest end or below the range of modern lherzolites.

The amphibole harzburgites, olivine hornblendites and hornblendites from the Cape Uivak layered body have distinctive HSE patterns distinguishing them from other Saglek ultramafics. Although the three lithologies have characteristic Pt and Pd abundances, almost all samples display Ru-enrichment relative to other IPGE, manifest as higher Ru/Ir and Ru/Os ratios than those in other groups of ultramafics (Fig. 5C). Similar Ru-enriched patterns were recognised in metaperidotites and massive chromitites from the Ujaragssuit nunât layered intrusion, which is located ~20 km south of Isua supracrustal belt in southwest Greenland (Coggon et al., 2015), which has a well-constrained minimum age of 3.811 Ga (Nutman et al., 1996). These ultramafics show the positive correlation between whole-rock IPGE abundances and modal proportion of chromite, suggesting that chromite and/or sub-micrometric inclusions in chromite host a significant portion of the Os, Ir and Ru (Coggon et al., 2015). Although stratiform chromitites are not recognised in the Cape Uivak layered body, the positive correlation between whole-rock IPGE and Cr abundances (Fig. 6) indicates that spinel/chromite or their inclusions play an important role in the Os-Ir-Ru budget (e.g., Righter et al., 2004; Brenan et al., 2012) as with the Ujaragssuit nunât layered intrusion. By contrast, the ultramafic rocks from the two Eoarchean layered bodies exhibit contrasting Re abundances; all lithologies found in Cape Uivak are depleted in Re characterised by low Re/Pd ratios unlike the Ujaragssuit nunât metaperidotites which have much higher Re abundances and Re/Pd ratios (Fig. 5C).

The HSE patterns for the metakomatiite suite in the Saglek ultramafics are relatively flat to slightly fractionated between IPGE and PPGE (Fig. 5D), similar to those of typical komatiite lavas (e.g., Fiorentini, 2011; Puchtel et al., 2014). One of the unique

characteristics observed in the Saglek metakomatiites is the strong depletion of Re relative to other HSE. This depletion seems unlikely to be primary, when considering that Re is the most-fluid mobile element among the HSE we analysed. Although the extent of Re depletion does not show any systematic variation against alteration indices such LOI values, the sample KC87-111I, which has the highest LOI value also the most depleted in Pd. By contrast, a metabasaltic komatiite (KC87-115D) does not show such obvious depletion in Re, and is characterised by smoothly fractionated HSE pattern with abundances slightly lower than metakomatiites (except for Re). The mobility of each HSE due to post-magmatic loss or gain will be further evaluated in terms of the Re-Os isotope systematics and covariations with other elements.

4.3. Re-Os isotope systematics

The Re-Os isotopic data for the whole rock samples of Saglek ultramafics are presented in Table 3 and plotted on Re-Os isochron diagrams in Fig. 7. Both Re depletion T_{RD} age (Walker et al., 1989) and T_{MA} model age (Allègre and Luck, 1980) were calculated using a ^{187}Re decay constant $\lambda = 1.666 \times 10^{-11}$ year^{-1} (Smoliar et al., 1996) relative to the evolution of average chondrite with initial $^{187}Os/^{188}Os = 0.09531$ at 4.558 Ga, and $^{187}Re/^{188}Os = 0.40186$ (Shirey and Walker, 1998) following the recommendation of Puchtel et al. (2014).

Similar to other Eoarchean ultramafic rocks previously analysed, Saglek ultramafic rocks display a large variation of $^{187}Os/^{188}Os$ ratios ranging from ~0.102 to 0.399. The most radiogenic and unradiogenic samples belong to metakomatiite suites; metabasaltic komatiite (KC87-115D) yields the highest $^{187}Re/^{188}Os$ of 5.58 and $^{187}Os/^{188}Os$ of 0.3992 (Fig. 7A), whereas three of five metakomatiites (KC87-111G, KC87-111I and KC87-111K) have the most unradiogenic $^{187}Os/^{188}Os$ values ranging from 0.1023 to 0.1037 among the studied samples. All of the unradiogenic samples scatter around a 3.6-Ga reference isochron assuming chondritic source (Fig. 7B), that agree well with their T_{MA} model ages (=3.57-3.64 Ga). Sample KC87-111E, one of the metakomatiites showing supra-chondritic $^{187}Os/^{188}Os$ values, gives similar T_{MA} ages (3.55 and 3.64 Ga) to those of unradiogenic metakomatiites, supporting their age significance and broadly closed system behaviour. Nine data points obtained from the four metakomatiites define a slope corresponding to an age of 3612 ± 130 Ma and an initial $^{187}Os/^{188}Os = 0.10200 \pm 18$ (MSWD = 40; Fig. 7C). Sample KC87-111F plots to the left of the errorchron likely due to the recent removal of Re.

The majority of samples from the lithospheric mantle suite show unradiogenic $^{187}Os/^{188}Os$ values ranging from 0.1041 to 0.1079, that are systematically higher than those of unradiogenic metakomatiites (Fig. 7B). Unlike the unradiogenic metakomatiites, the lithospheric mantle suites scatter widely on the isochron plot. Three data points from the two dunite samples (KC91-21A and B) having elevated $^{187}Re/^{188}Os$ provide T_{MA} model ages of 3.56-3.99 Ga overlapping with or older than the T_{MA} ages of metakomatiite. However, these old T_{MA} ages could be erroneous and likely reflect recent addition of Re. With the exception of these two dunites and two hornblendites from the Cape Uivak (KC91-21C-2 and 4), the lithospheric mantle suite yields Paleoproterozoic to Mesoarchean Os model ages (T_{MA}) of 2.30-3.43 Ga, with a similar range for T_{RD} model ages (T_{RD} = 2.79-3.33 Ga for unradiogenic samples).

Although open-system behaviour of the Re-Os isotope systematics is evident in the lithospheric mantle suite, a subset of amphibole-rich samples studied by Collerson et al. (1991) and Wendt and Collerson (1999) for ^{147}Sm-^{143}Nd and Pb-Pb systematics (KC87-102, KC87-106A, KC-87-114G, KC-87-114K, KC-87-114I and KC87-119A) defines a scattered correlation on the Re-Os isochron diagram corresponding to an age of 3053 ± 130 Ma, an initial $^{187}Os/^{188}Os$ of 0.1046 ± 0.0012, and an MSWD = 219 (dashed line in Fig. 7D). The scatter is reduced somewhat if the data points from sample KC87-114K are excluded for the regression (MSWD = 10.2) but the age (3096 ± 170 Ma) and the initial $^{187}Os/^{188}Os$ (0.1041 ± 0.0017, Fig. 7D) are not significantly different. However, we note that these correlations are largely controlled by five replicates of KC87-119A showing T_{MA} model ages ranging from 2.64 to 3.17 Ga.

5. Discussion

5.1. Ages of the Saglek ultramafics

As inferred from some scattering in the Re-Os isochron plot, secondary processes may have affected not only lithophile trace elements but also the less mobile HSE. Thus, in order to address the HSE characteristics of the Early Archean mantle in general, we need to evaluate the degree to which secondary processes have impacted the HSE compositions of each suite of the Saglek ultramafics. This can potentially be assessed by examining age information obtained by previous studies and the Re-Os isotope systematics.

Previous studies have demonstrated that the whole rock compositions of the metakomatiite suite of Saglek ultramafics were not significantly disrupted by secondary processes, based mainly on the good agreement of ^{147}Sm-^{143}Nd and Pb-Pb whole rock ages

of 4017 ± 194 Ma (MSWD = 24) and 3845 ± 160 Ma (MSWD = 9.75), respectively (Collerson et al., 1991; Wendt and Collerson, 1999). This Eoarchean age has recently been confirmed by the coupled ^{146}Sm-^{142}Nd and ^{147}Sm-^{143}Nd study of the new sample set from the Saglek region, which yields a more precise ^{147}Sm-^{143}Nd age of 3782 ± 93 Ma (MSWD =15) with initial ^{143}Nd/^{144}Nd = 0.50780 ± 0.00003 ($\varepsilon^{143}Nd_i$ = 1.4 ± 0.6) for samples carrying positive ^{142}Nd anomalies (Morino et al., 2017). These ages are slightly older than the Re-Os isotope age of 3612 ± 130 Ma (MSWD = 40) obtained by regression through nine analyses from four metakomatiites, but agree, within error, of the Pb-Pb and the latest ^{147}Sm-^{143}Nd ages. The Re-Os chronological data is potentially erroneous because of Re gain or loss due to secondary processes, which is evident at least for two samples KC87-115D and KC87-111F, which scatter well below and above the 3612 Ma errorchron, respectively. All metakomatiites show variable Re depletions relative to Pd when compared to the reconstructed HSE compositions for primary komatiites (Emplaced komatiite lava in Fig. 5D; Puchtel et al., 2014). Samples KC87-115D and KC87-111F define the highest and lowest Re/Pd ratios among the metakomatiite suite. It therefore seems possible that Re concentrations in studied metakomatiites have been significantly affected by post Eoarchean processes such as high-grade metamorphism at around 2.8-2.9 Ga, resulting in a small displacement of the regressions toward a younger age.

However, the close agreement between the Re-Os errorchron and T_{MA} ages (=3.55-3.64 Ga) obtained by excluding the two Re-disturbed samples may suggest an alternative explanation that the Re-Os system yields more accurate age of magmatic emplacement of the metakomatiites than those from Sm-Nd and Pb-Pb systematics. Since lithophile trace elements are depleted in a high degree melt such as komatiite and are particularly vulnerable to contamination effects during syn- and/or post-magmatic processes (e.g., Lahaye et al., 1995), anomalously old ages due to incorporation of older crustal components have been frequently reported for combined Sm-Nd and Pb-Pb systematics of komatiites (e.g., Chauvel et al., 1985; Juteau et al., 1988). Indeed, Saglek metakomatiites display slightly elevated LREE and pronounced Pb enrichment relative to neighbouring elements on the PM-normalised diagram (Fig. 4A and C), implying that at least the Pb isotopic signature of the mantle component was overwhelmed by that of crustal materials. On the other hand, the Re-Os isotope systematics of the komatiite system are virtually impervious to the effects of crustal contamination and hydrothermal alteration as a consequence of much higher Os abundances in the komatiitic magma relative to surrounding crust or hydrothermal fluid. Although such post-magmatic processes often resulted in scattering of Re data in Archean komatiite systems, the Re-Os isotope

systematics of the Archean komatiites typically yield magmatic emplacement ages because Re gain or loss were nearly contemporaneous with the lava emplacement (e.g., Puchtel et al., 2014).

The same arguments made for the metakomatiites can also apply to the lithospheric mantle suite for explaining the substantial discrepancy in the age information obtained from Sm-Nd, Pb-Pb and Re-Os systematics. The highly scattered Re-Os data in isochron diagram leaves little doubt about the open-system behaviour of this system in the lithospheric mantle suite. However, we interpret that the poorly correlated Pb-Pb and Re-Os errorchrons (2907 ± 560 Ma and 3053 ± 130 Ma, respectively) for amphibole-rich variants of the lithospheric mantle rocks are in agreement each other, and approximate the timing of metasomatic redistribution of Re and U during the ~2.8-2.9 Ga metamorphic event. Indeed, the Isua ultramafic rocks studied by Rizo et al. (2016b) define a Re-Os errorchron corresponding to an age of 2.82 ± 0.33 Ga with the initial $^{187}Os/^{188}Os$ ratio of 0.1007 ± 0.0011, which is identical to the chondritic $^{187}Os/^{188}Os$ ratio at 3.7-3.8 Ga. This can be interpreted as representing the age of metamorphic redistribution of Re while revealing the inheritance of primary Os isotope signatures, presumably under amphibolite facies conditions. In contrast, the significance of the considerably older Sm-Nd isochron of 3815 ± 121 Ma (MSWD = 2.6) compared to Pb-Pb and Re-Os ages reported for the same sample set remains uncertain, but this appears to be a result of mixing produced at the time of protolith formation or during the regional 2.8-2.9 Ga metamorphic event for the following two reasons.

First, both amphibole-rich and olivine-rich variants (mainly dunites) of the lithospheric mantle suites are dominated by Mesoarchean Os model ages, either T_{MA} or T_{RD} (T_{MA} = 2.30-3.43 Ga, excepting sample KC91-21A and B with clear Re enrichment; T_{RD} = 2.79-3.33 Ga; Table 4). Although their exact origins need to be rigorously evaluated, the systematic HSE patterns of dunites that have flat IPGEs and a strong depletion in PPGE are consistent with their low Al_2O_3 contents and other potential indices of melt depletion and hence with an origin as restites from high degrees of melt extraction. Even if they originated from other processes such as olivine accumulation from a melt (a cumulate origin) or pyroxene dissolution in a migrating Si-undersaturated melt through peridotite matrix (melt-rock interaction origin; e.g. Kelemen et al., 1995), it is likely that the low Re/Os ratios of these dunites were acquired during their formation, and the retarded ingrowth of ^{187}Os resulted in non-radiogenic Os isotope compositions. If their long-term evolution with low Re/Os ratios is correct, their Os model ages, either T_{MA} or T_{RD}, provide reasonable approximations of the age of dunite formation. Although it seems possible that significant Re loss associated with

the ~2.8-2.9 Ga metamorphic event may have resulted in variable Os model ages, the close agreement between maximum T_{MA} and T_{RD} indicate that the dunite formation occurred around 3.3-3.4 Ga and subsequent metasomatism on dunites or possibly harzburgites created amphibole-rich variants of the lithospheric mantle suites.

Second, a group of ultramafic rocks, without resolvable ^{142}Nd anomalies, studied by Morino et al. (2017) yield a whole-rock ^{147}Sm-^{143}Nd isochron age of 3362 ± 100 Ma (MSWD = 4.5) in agreement with the Mesoarchean Os model ages of the lithospheric mantle suite (3.3-3.4 Ga). In contrast to our interpretation of their mantle origin, Morino et al. (2017) claimed that the ultramafics they studied represent Mesoarchean komatiites associated with Upernavik supracrustal groups, despite the fact that the major and trace element variations of these rocks are broadly consistent with the amphibole-rich variants of the lithospheric mantle suite presented here (Figs. 3 and 4). Although current evidence is not definitive, we consider that the REE systematics of these rocks and the observed age discrepancies can be accounted for if they were a series of metasomatised mantle rocks. One of the most characteristic features shared by these ultramafics (including dunites) is the common presence of pronounced negative Eu anomalies. This strongly suggests that addition of externally derived melts/fluids or assimilation of older crustal materials are responsible for a significant fraction of LREE and, consequently, the interpretation of ^{147}Sm-^{143}Nd systematics is not straightforward. It is interesting to note that the magnitude of Eu anomalies tends to decrease with increasing absolute REE abundances (Fig. 4A and B). This cannot be attributed to either a simple bulk mixing or more complex AFC processes involving typical continental crust-like assimilant with negative Eu anomalies. However, a likely explanation is that infiltration of fluids/melts having negative Eu anomalies into mantle rocks creates a series of melting residues, and subsequent metasomatic overprints involving amphibole crystallization mask pre-existing Eu anomalies due to total REE increase. If this explanation is sound, it seems likely that the ^{147}Sm-^{143}Nd isochron provides the timing of flux melting and amphibole crystallisation, which proceed contemporaneously (3362 ± 100 Ma; Morino et al., 2017), but the incorporation of less altered/metasomatised samples with higher ε^{143}Nd displace the isochron toward older ages (3815 ± 121 Ma; Collerson et al., 1991).

Given these considerations, the exact timing of protolith formation for both metakomatiite and lithospheric mantle suites is still an open question. However, we envisage that komatiite emplacement in the Eoarchean Saglek terrain is firmly constrained by the agreement between Sm-Nd, Pb-Pb and Re-Os chronological data (~3.6-3.8 Ga). Mesoarchean formation of lithospheric mantle suite (~3.3-3.4 Ga) is also loosely

constrained by the agreement of Os model ages and the recently obtained ^{147}Sm-^{143}Nd isochron. Regardless of the exact reason for the age discrepancies, however, the present Os isotope study supports the previous interpretation from Sm-Nd and Pb-Pb isotope studies that the two ultramafic suites are not coeval and experienced contrasting histories during their evolution (Collerson et al., 1991; Wendt and Collerson, 1999; Morino et al., 2017). Moreover, our present results lend support for previous notion that the two ultramafic suites are associated with the distinct supracrustal units distributed over the Saglek/Hebron area in Labrador: the metakomatiites belong to the Eoarchean Nulliak assemblage, whereas the lithospheric mantle rocks occur only in relation to Mesoarchean Upernavik supracrustal groups (Morino et al., 2017). However, further detailed geological and geochronological studies are clearly required to evaluate this possibility and its tectonic significance, in particular in improving the veracity of the geochronology for all systems on these complex metamorphic rocks.

5.2. HSE characteristics of the source mantle

In the section above, for convenience, we utilised Re-Os model ages calculated assuming chondritic evolution of the mantle source reservoirs of the Labrador ultramafics. This assumption is widely accepted in order to use age information from Phanerozoic to Proterozoic sample suites because the HSEs are thought to be present in broadly chondritic proportions in the primitive upper mantle (PUM) - generally used as a proxy for the whole mantle estimated by projection techniques for variably depleted peridotites from worldwide locations (Meisel et al., 2001; Becker et al., 2006). However, as there is significant inherent uncertainty as to when and how PUM-like mantle was established, the accuracy of Os model age of the Labrador ultramafics depends on how much of the Archean mantle had chondritic relative abundances of HSEs. Well-resolved ^{182}W isotope anomalies, relative to the present day mantle, in Eoarchean terrestrial rocks have been attributed to the wide-spread preservation of mantle domains that escaped some inputs from late accretion of chondritic materials (Willbold et al., 2011; Willbold et al., 2015; Dale et al., 2017). In addition, an apparent time-dependent enrichment trend in HSE abundances of Archean to Proterozoic komatiites has been interpreted to reflect the protracted homogenisation of late accreted chondritic materials into deeper portions of Earth's mantle (Maier et al., 2009; Fiorentini et al., 2011). In order to address whether the Saglek ultramafic suites were derived from such mantle domains - less affected by late accretion - as implied by their uniform ~+11 ppm enrichments in ^{182}W (Liu et al., 2016), we apply our HSE data to constrain source mantle characteristics.

Figure 7 shows covariations of major elements and abundance ratios of two HSE of differing compatibility. During komatiite lava differentiation, incompatible/compatible HSE ratios are expected to increase with degree of fractionation. Both Pd/Ir and Pt/Ir ratios of the metakomatiites show broad positive correlations against Al_2O_3 contents (Fig. 7A and B). These correlations are consistent with their generation during crystallization of sulphur-undersaturated komatiite magma (e.g., Puchtel and Humayun, 2001), although significant offsets are observed in high-Al_2O_3 samples, presumably due to sulphide saturation. As with the metakomatiites, dunites in the lithospheric mantle suite show positive correlations of Pd/Ir and Pt/Ir against Al_2O_3 content diagrams consistent with the idea that incompatible/compatible HSE ratios decrease with degree of melt extraction (e.g., Pearson et al., 2004; Aulbach et al., 2015). Interestingly, on both diagrams, regression lines through the two ultramafic suites are characterised by different slopes, but seem to intersect at close to PUM values, indicating that they were derived from a similar source mantle having broadly chondritic HSE ratios, but different processes, namely fractional crystallization and partial melting, are responsible for PPGE/IPGE fractionation.

In contrast to PPGE/IPGE ratio trends, the variation of Ru/Ir and Ru abundances against MgO is far more scattered (Figs. 8C and D). Ruthenium is known to be less incompatible than Pd and Pt, and less compatible than Ir and Os during differentiation of typical komatiite lava (e.g., Puchtel et al., 2014). On the other hand, IPGE inter-element fractionation is usually very minor through a range of mantle melting, even to the high degrees of melting, well beyond sulphide exhaustion (Pearson et al., 2004; Mungall and Brenan, 2014). Consistent with this, the data from the two Labrador ultramafic suites tend to follow a broad trend with negative slope on the Ru/Ir versus MgO diagram (Fig. 8C). It is striking that the majority of data plot in the field of suprachondritic Ru/Ir ratios, and that the broad trend passes through the PUM estimate. The observed Ru excess does not reflect selective Ru enrichments in these rocks because their Ru abundances tend to be lower than the PUM value (Fig. 8D). Indeed, they display somewhat coherent behaviour against MgO as with other Archean komatiites and cratonic peridotites. Moreover, three data points of the Isua ultramafics, which provide the most robust mantle estimate for ~3.8 Ga Isua source due to their mantle-like HSE patterns and MgO contents (Dale et al., 2017), share the same HSE characteristics with suprachondritic Ru/Ir ratios and lower-than PUM Ru concentrations. Judging from these observations, we envisage that a PUM-like (in relative HSE abundances) but slightly HSE-poor source mantle contributed to the generation of the two suites of Saglek ultramafics, despite their contrasting ages and presumably environments of formation.

The origin of the suprachondritic Ru/Ir and possibly Pd/Ir ratios evident in most estimates of PUM is somewhat unclear, partly because of the fact that the HSE compositions of PUM were estimated from variably depleted peridotites (Becker et al., 2006). Thus, several studies have raised questions about the significance of apparent non-chondritic ratios of PUM, and argued that the true composition of PUM, prior to complex processing within the mantle, would be chondritic (Rehkämper et al., 1999; Alard et al., 2000; Lorand et al., 2009). However, a growing database of HSE abundances in natural peridotites from highly diverse locations, of variable age, suggest that suprachondritic Ru/Ir and Pd/Ir ratios appear to be a robust and ubiquitous characteristics of the Earth's upper mantle, rather than a reflection of elemental redistribution caused by regionally specific processing (e.g., Day et al., 2017).

At present, two competing hypotheses have been proposed for explaining the suprachondritic Ru/Ir and Pd/Ir ratios of PUM. One is that it originated in a late accretionary component, partly comprised of materials outside of the range of the current dataset of chondrites, as inferred from studies of HSE in lunar impact melt rocks and breccias (Puchtel et al., 2008; Fischer-Gödde and Becker, 2012; Sharp et al., 2014; Liu et al., 2015). These studies identified that some impactors involved in basin-forming events on the Moon during the period of late heavy bombardment (~4.1-3.8 Ga) had fractionated HSE compositions showing higher Ru/Ir and Pd/Ir than known chondrites. Regardless of the origin of such impactors with fractionated HSE (early solar system bodies with unknown compositions or evolved metallic materials from a fractionated planetesimal core), this model implies that similar materials contributed to the HSE budget of the silicate Earth as part of the late accretionary inventory. The other is that it remained in the mantle after a 2 stage core formation process, involving late stage sulphide segregation from a magma ocean to the Earth's core followed by a late accretion (CI chondrite-like), recently proposed based on metal-silicate and sulphide-silicate partitioning experiments examining the effect of sulphur on the behavior of the HSEs during core formation (Laurenz et al., 2016). The model assumes that, after the main episode of core formation under S-free and reducing conditions, a Moon-forming impact caused by accretion of oxidised and volatile-rich material to the proto-Earth inducing segregations of S-bearing metal and FeS sulphide melt in a cooling magma ocean. Since Ru and Pd are less chalcophile than Pt and Ir at high P–T, PUM-like HSE abundances can be well reproduced, if a certain amount of CI-like materials was accreted before (~1%) and after (~0.4%) the sulphide segregation.

The former and the latter hypotheses would respectively predict less and more fractionated HSE patterns for pre-late accretionary mantle compared to PUM estimates. Discrimination between the two hypotheses is potentially possible from the HSE characteristics of late veneer-poor mantle. In this regard, our HSE data suggest that the mantle sources for the ~3.6-3.8 Ga metakomatiites and ~3.3-3.4 Ga lithospheric mantle suites of Labrador ultramafics, both associated with uniform ~+11 ppm enrichments in ^{182}W relative to the Earth's modern mantle (Liu et al., 2016), are not completely devoid of late accretionary components, but it is possible that they received less addition of late accreted material (partial late veneer) by analogy with the proposal for the ~3.8 Ga Isua source mantle that shows a 13 ± 4 ppm ^{182}W excess coupled with some HSE deficiencies (Dale et al., 2017). However, a fundamental question raised by our data is whether such mantle domains persisted over the entire period of Eoarchean. One explanation for this is that ^{182}W enrichments were not derived from sources depleted in HSEs (e.g., Rizo et al., 2016b), or that the decoupling between ^{182}W and HSEs were caused by significant secondary W mobility (e.g., Touboul et al., 2014). The former would be consistent with the occurrence of positive ^{142}Nd anomalies in the Eoarchean suite of Saglek ultramafics, implying that these two extinct radionuclide isotope systems reflect early Earth differentiation (Morino et al., 2017). The latter would also be consistent with the observation that W in the Saglek ultramafics is largely hosted in secondary grain-boundary assemblages coupled with significant enrichments of W relative to elements with similar incompatibilities (Liu et al., 2016). Hence, these observations do not allow meaningful implications to be made regarding the feasibility of "partial late veneer hypothesis" and the origin of suprachondritic Ru/Ir and Pd/Ir ratios of current PUM estimate. However, unlike the ^{182}W signature, similar HSE characteristics between ~3.6-3.8 Ga and ~3.3-3.4 Ga in the Saglek ultramafic sources is unlikely to be attributed to secondary HSE mobility, and may place important constraints on the Archean convecting mantle in general.

5.3. Implications for the Archean convecting mantle

Figure 9A displays the temporal changes of initial ^{187}Os/^{188}Os in the sources of Archean komatiite systems, compared with the data from Saglek, Nuvvuagittuq, Isua, and Ujaragssuit nunât. Since the exact ages of formation for the Saglek lithospheric mantle and metakomatiite suites are not well constrained, possible ranges deduced from ^{187}Re-^{187}Os and ^{147}Sm-^{143}Nd chronometry are illustrated in addition to ages and initial ^{187}Os/^{188}Os derived from whole rock errorchrons. Most Archean komatiites, including Saglek metakomatiites presented in this study, have initial ^{187}Os/^{188}Os ratios that broadly follow the chondritic

evolution trend, consistent with the contention that the HSE compositions of komatiite sources are generally chondritic in relative abundances. It is known that a present-day $^{187}Os/^{188}Os$ value for PUM of 0.1296, deduced from world-wide peridotites with deletion age of <2.0 Ga (Meisel et al., 2001), is slightly more radiogenic than the average $^{187}Os/^{188}Os$ of 0.1270 for carbonaceous, ordinary and enstatite chondrites (Walker et al., 2002). The same conclusion is reached even if the larger compilation of chondritic values including newly obtained data is considered (the range is 0.124-0.130 with some outliers: Day et al., 2016a). However, the difference in the two evolution trajectories is minor in the Archean period. Thus to a first order, indistinguishable $^{187}Os/^{188}Os$ in the vast majority of Archean komatiite sources and the PUM trajectory representing <2.0 Ga upper mantle indicates that the terrestrial mantle has no major, global-scale variation in Re-Os compositions in time and space, particularly if komatiites can be regarded as melting products of deep mantle upwelling or plumes originated from lower mantle.

Small but resolvable offsets to higher $^{187}Os/^{188}Os$ ratios observed in some localities can be attributed to one of several causes: (1) Radiogenic Os from earlier crustal materials were incorporated into magmas or source mantles; (2) The presence of ancient mantle domains that underwent core separation and magma ocean fractionation processes, or were subsequently incompletely mixed with incoming accreted material, may have persisted during the Archean period; (3) Secondary effects such as metamorphic and metasomatic processes may have led to the overestimation of initial $^{187}Os/^{188}Os$ ratios and/or ages of rock formation. It has been proposed that the first of these scenarios is likely the process responsible for the observed $^{187}Os/^{188}Os$ offsets in 3.71 Ga boninite-like metabasalts from the Isua supracrustal belt (Frei et al., 2004) and in komatiitic basalts from the 2.4 Ga Vetreny belt, Fennoscandian Shield (Puchtel et al., 2016b). In contrast the presence of ancient domains with more radiogenic Os has been invoked for the 2.8 Ga Kostomuksha komatiites, Russia (Puchtel and Humayun, 2005) and the 3.55 Ga Schapenburg komatiites, South Africa (Puchtel et al., 2009a), constrained by data from short-lived ^{182}Hf-^{182}W and ^{146}Sm-^{142}Nd systems (Touboul et al., 2012; Puchtel et al., 2016a). Since robust isochrons are rarely observed in the Re-Os data for Eoarchean rocks, instead of calculating initial $^{187}Os/^{188}Os$ ratios from measured $^{187}Re/^{188}Os$ ratios, the lowest present-day $^{187}Os/^{188}Os$ from each locality and sample types are plotted in Fig. 9A (except for Isua boninites). As demonstrated in the previous section, we consider that the large apparent range of initial $^{187}Os/^{188}Os$ in Saglek lithospheric mantle suites relate to uncertainties in their ages of formation and to secondary Re mobility. Probably the same is true for other Eoarchean

ultramafic rocks. It is therefore difficult to address extents of $^{187}Os/^{188}Os$ isotope heterogeneity in the Eoarchean mantle from current datasets. However, the good agreement between the lowest $^{187}Os/^{188}Os$ recorded in an Isua ultramafic rock (sample 460000; Frei and Jensen, 2003) and the chondritic evolution line at 3.81 Ga supports the observation from studies of komatiites that the terrestrial mantle had a limited variation in $^{187}Os/^{188}Os$ ratio during the entire Archean.

Perhaps the most enigmatic characteristics of the Archean convecting mantle is that, despite its almost identical $^{187}Os/^{188}Os$ evolution to that of PUM, the HSE abundances estimated from komatiites are strikingly lower than the PUM estimates, ranging from 27 ± 4 % in the 3.55 Ga Schapenburg komatiites to 85 ± 5 % in the 2.72 Ga Abitibi komatiites (expressed by total Pt + Pd in their sources relative to PUM; Puchtel et al., 2009a; Puchtel et al., 2009b). Maier et al. (2009) have proposed that gradual downward mixing of a late veneer of chondritic impactors into the mantle can account for the apparent increase in the HSE abundances of komatiite sources with time. However, Puchtel et al. (2016b) concluded that secular increase in HSE abundances is not recognisable in komatiite sources from 3.5 to 2.4 Ga. To address this issue, the reconstructed Ru abundances of komatiite sources reported by Puchtel and Humayun (2005) and Puchtel et al. (2007, 2009a, 2009b, 2014) are compared with the estimated values and ranges in Ru abundance in the sources of the Saglek ultramafic suites (Fig. 9B). For their estimation, we assumed that the bulk solid-liquid partition coefficient for Ru was close to unity during high degrees of partial melting and komatiite differentiation, as applied to other komatiite systems. This value is consistent with the Ru behaviour documented by studies of komatiite lavas (e.g., 0.96-1.4; Puchtel et al., 2004) and experimentally determined olivine-melt partition coefficients for Ru (D_{Ru} = 0.5-2; Brenan et al., 2003). We adopted the observed ranges of Ru concentrations in high-MgO metakomatiites and dunites (>25 wt.%) as being equal to their source variations. This estimation provides a Ru concentration for the Saglek metakomatiite source with a range of 4.1-7.2 ppb and an average of 5.2 ± 1.3 ppb (1σ), whereas the source mantle for dunites has a Ru content with a range of 4.1-6.3 ppb and an average of 5.7 ± 0.7 ppb (1σ). These average Ru concentrations, translated as 74 ± 18% and 82 ± 10% of the PUM estimate, are virtually identical to the Ru content estimated for ~3.8 Ga Isua source (5.1 ± 0.8 ppb equal to 73 ± 12% of PUM estimate) and those of the majority of late Archean komatiites (Volotsk, Abitibi, Belingwe and Kostomuksha) and ~3.3 Ga Weltevreden komatiite (5.6-6.0 ppb equal to 80-86% of PUM estimate). This demonstrates that lower HSE abundances (~70-86% of PUM) are not unique to the sources

of komatiites, but rather might be a ubiquitous feature of Archean convecting mantle. Although this is consistent with the observations from the compilation of kimberlite-borne cratonic xenoliths (Aulbach et al., 2015), full resolution of this issue will have to wait for work on new discoveries because the data from Archean ultramafic rocks are still scarce. Further studies on HSE abundances in Archean rocks together with updating and re-assessment of PUM abundances may provide an important opportunity to test whether sluggish mixing of the late accretionary component played a role in forming the contrasting HSE abundances between Archean convecting mantle and those of PUM - representing the modern convecting mantle.

Acknowledgments

We are grateful to Ryoko Senda, Hideo Yamamoto, Yukari Otsuki, Sanae Senshu for their assistance with sample preparation and chemical analyses at JAMSTEC, and Masanori Shimojo, and Keiko Koshida at the University of Tokyo. Guillaume Caro, James Day, an anonymous reviewer and the associate editor, Frédéric Moynier are also thanked for their careful constructive reviews. This study was partially supported by the JSPS KAKENHI Grant Numbers JP21840068, JP26220713, JP15H05830.

References

Alard, O., Griffin, W.L., Lorand, J.-P., Jackson, S.E., O'Reilly, S.Y., 2000. Non-chondritic distribution of the highly siderophile elements in mantle sulphides. *Nature* **407**, 891-894.

Albarede, F., 2009. Volatile accretion history of the terrestrial planets and dynamic implications. *Nature* **461**, 1227-1233.

Allègre, C.J., Luck, J.-M., 1980. Osmium isotopes as petrogenetic and geological tracers. *Earth Planet. Sci. Lett.* **48**, 148-154.

Anders, E., Grevesse, N., 1989. Abundances of the elements: Meteoritic and solar. *Geochim. Cosmochim. Acta* **53**, 197-214.

Arndt, N., Lesher, M., Barnes, S.J., 2008. Komatiite. Cambridge University Press, Cambridge, U.K. Cambridge University Press, Cambridge, U.K.

Aulbach, S., Mungall, J.E., Pearson, D.G., 2015. Distribution and processing of highly siderophile elements in cratonic mantle lithosphere. *Reviews in Mineralogy & Geochemistry* **81**, 239-245.

Barnes, S.J., Fiorentini, M.L., 2008. Iridium, ruthenium and rhodium in komatiites: Evidence for iridium alloy saturation. *Chem. Geol.* **257**, 44-58.

Becker, H., Horan, M.F., Walker, R.J., Gao, S., Lorand, J.-P., Rudnick, R.L., 2006. Highly siderophile element composition of the Earth's primitive upper mantle: constraints from new data on peridotite massifs and xenoliths. *Geochim. Cosmochim. Acta* **70**, 4528-4550.

Bennett, V.C., Nutman, A.P., Esat, T.M., 2002. Constraints on mantle evolution from $^{187}Os/^{188}Os$ isotopic compositions of Archean ultramafic rocks from southern West

Greenland (3.8 Ga) and Western Australia (3.46 Ga). *Geochim. Cosmochim. Acta* **66**, 2615-2630.

Birck, J.-L., Roy Barman, M., Capmas, F., 1997. Re-Os isotopic measurements at the femtomole level in natural samples. *Geostand. Newsl.* **21**, 19-27.

Borg, L.E., Connelly, J.N., Boyet, M., Carlson, R.W., 2011. Chronological evidence that the Moon is either young or did not have a global magma ocean. *Nature* **477**, 70-U150.

Brenan, J.M., McDonough, W.F., Dalpé, C., 2003. Experimental constraints on the partitioning of rhenium and some platinum-group elements between olivine and silicate melt. *Earth Planet. Sci. Lett.* **212**, 135-150.

Brenan, J.M., Finnigan, C.F., McDonough, W.F., Homolova, V., 2012. Experimental constraints on the partitioning of Ru, Rh, Ir, Pt and Pd between chromite and silicate melt: The importance of ferric iron. *Chem. Geol.* **302–303**, 16-32.

Bridgewater, D., Collerson, K.D., Hurst, R.W., Jesseau, C.W., 1975. Field characters of the early Precambrian rocks from Saglek, Coast of Labrador. *Pap. Geol. Surv. Canada* **74-1a**, 287-296.

Bridgewater, D., Collerson, K.D., 1976. The major petrological and geochemical characters of the 3,600 m.y. Uivak Gneisses from Labrador. *Contibutions to Mineralogy and Petrology* **54**, 43-59.

Bridgwater, D., Schiøtte, L., 1991. The Archean gneiss complex of northern Labrador: a review of current results, ideas and problems. *Bulletin of the Geological Society of Denmark* **39**, 153-166.

Chatterjee, R., Lassiter, J.C., 2016. 186Os/188Os variations in upper mantle peridotites: Constraints on the Pt/Os ratio of primitive upper mantle, and implications for late veneer accretion and mantle mixing timescales. *Chem. Geol.* **442**, 11-22.

Chauvel, C., Dupré, B., Jenner, G.A., 1985. The Sm-Nd age of Kambalda volcanics is 500 Ma too old! *Earth Planet. Sci. Lett.* **74**, 315-324.

Chou, C.-L., 1978. Fractionation of siderophile elements in the Earth's upper mantle. *Proc. Lunar Planet. Sci. Conf. 9th* 219–230.

Coggon, J.A., Luguet, A., Fonseca, R.O.C., Lorand, J.-P., Heuser, A., Appel, P.W.U., 2015. Understanding Re–Os systematics and model ages in metamorphosed Archean ultramafic rocks: a single mineral to whole-rock investigation. *Geochim. Cosmochim. Acta* **167**, 205-240.

Cohen, A.S., Waters, F.G., 1996. Separation of osmium from geological materials by solvent extraction for analysis by thermal ionisation mass spectrometry. *Anal. Chim. Acta* **332**, 269-275.

Collerson, K.D., Kerr, A., Vocke, R.D., Hanson, G.N., 1982. Reworking of sialic crust as represented in late Archean–age gneisses, northern Labrador. *Geology* **10**, 202-208.

Collerson, K.D., McCulloch, M.T., Bridgwater, D., 1984. Nd and Sr isotopic crustal contamination patterns in an Archaean meta-basic dyke from northern Labrador. *Geochim. Cosmochim. Acta* **48**, 71-83.

Collerson, K.D., Campbell, L.M., Weaver, B.L., Palacz, Z.A., 1991. Evidence for extreme mantle fractionation in early Archean ultramafic rocks from northern Labrador. *Nature* **349**, 209-214.

Connolly, B.D., Puchtel, I.S., Walker, R.J., Arevalo, R., Jr., Piccoli, P.M., Byerly, G., Robin-Popieul, C., Arndt, N., 2011. Highly siderophile element systematics of the 3.3 Ga Weltevreden komatiites, South Africa: Implications for early Earth history. *Earth Planet. Sci. Lett.* **311**, 253-263.

Dale, C.W., Burton, K.W., Greenwood, R.C., Gannoun, A., Wade, J., Wood, B.J., Pearson, D.G., 2012. Late accretion on the earliest planetesimals revealed by the highly siderophile elements. *Science* **336**, 72-75.

Dale, C.W., Kruijer, T.S., Burton, K.W., 2017. Highly siderophile element and 182W evidence for a partial late veneer in the source of 3.8 Ga rocks from Isua, Greenland. *Earth Planet. Sci. Lett.* **458**, 394-404.

Day, J.M.D., Pearson, D.G., Taylor, L.A., 2007. Highly siderophile element constraints on accretion and differentiation of the Earth-Moon system. *Science* **315**, 217-219.

Day, J.M.D., Walker, R.J., Qin, L.P., Rumble, D., 2012. Late accretion as a natural consequence of planetary growth. *Nat. Geosci.* **5**, 614-617.

Day, J.M.D., Walker, R.J., 2015. Highly siderophile element depletion in the Moon. *Earth Planet. Sci. Lett.* **423**, 114-124.

Day, J.M.D., Brandon, A.D., Walker, R.J., 2016a. Highly siderophile elements in Earth, Mars, the Moon, and Asteroids. *Reviews in Mineralogy & Geochemistry* **81**, 161-238.

Day, J.M.D., Waters, C.L., Schaefer, B.F., Walker, R.J., Turner, S., 2016b. Use of Hydrofluoric Acid Desilicification in the Determination of Highly Siderophile Element Abundances and Re-Pt-Os Isotope Systematics in Mafic-Ultramafic Rocks. *Geostand. Geoanal. Res.* **40**, 49-65.

Day, J.M.D., Walker, R.J., Warren, J.M., 2017. 186Os–187Os and highly siderophile element abundance systematics of the mantle revealed by abyssal peridotites and Os-rich alloys. *Geochim. Cosmochim. Acta* **200**, 232-254.

Fiorentini, M.L., Rosengren, N., Beresford, S.W., Grguric, B., Barley, M.E., 2007. Controls on the emplacement and genesis of the MKD5 and Sarah's Find Ni–Cu–PGE deposits, Mount Keith, Agnew–Wiluna Greenstone Belt, Western Australia. *Mineralium Deposita* **42**, 847-877.

Fiorentini, M.L., 2011. Global variability in the platinum-group element contents of komatiites. *J. Petrol.* **52**, 83-112.

Fiorentini, M.L., Barnes, S.J., Maier, W.D., Burnham, O.M., Heggie, G., 2011. Global Variability in the Platinum-group Element Contents of Komatiites. *J. Petrol.* **52**, 83-112.

Fischer-Gödde, M., Becker, H., Wombacher, F., 2010. Rhodium, gold and other highly siderophile element abundances in chondritic meteorites. *Geochim. Cosmochim. Acta* **74**, 356-379.

Fischer-Gödde, M., Becker, H., Wombacher, F., 2011. Rhodium, gold and other highly siderophile elements in orogenic peridotites and peridotite xenoliths. *Chem. Geol.* **280**, 365-383.

Fischer-Gödde, M., Becker, H., 2012. Osmium isotope and highly siderophile element constraints on ages and nature of meteoritic components in ancient lunar impact rocks. *Geochim. Cosmochim. Acta* **77**, 135-156.

Frei, R., Jensen, B.K., 2003. Re-Os, Sm-Nd isotope- and REE systematics on ultramafic rocks and pillow basalts from the Earth's oldest oceanic crustal fragments (Isua Supracrustal Belt and Ujaragssuit nunât area, W Greenland). *Chem. Geol.* **196**, 163-191.

Frei, R., Polat, A., Meibom, A., 2004. The Hadean upper mantle conundrum: evidence for source depletion and enrichment from Sm-Nd, Re-Os, and Pb isotopic compositions in 3.71 Gy boninite-like metabasalts from the Isua supracrustal belt, Greenland. *Geochim. Cosmochim. Acta* **68**, 1645-1660.

Govindaraju, K., 1994. Compilation of working values and sample descriptions for 383 geostandards. *Geostandard Newsletters* **18**, 158 pp.

Hurst, R.W., Bridgewater, D., Collerson, K.D., 1975. 3600-m.y. Rb-Sr ages from very early Archean gneisses from Saglek Bay, Labrador. *Earth Planet. Sci. Lett.* **27**, 392-403.

Imai, N., Terashima, S., Itoh, S., Ando, A., 1995. 1994 Compilation of Analytical Data for Minor and Trace Elements in Seventeen Gsj Geochemical Reference Samples, "Igneous Rock Series". *Geostand. Geoanal. Res.* **19**, 135-213.

Ishikawa, A., Senda, R., Suzuki, K., Dale, C.W., Meisel, T., 2014. Re-evaluating digestion methods for highly siderophile element and ^{187}Os isotope analysis: evidence from geological reference materials. *Chem. Geol.* **384**, 27-46.

Jacobson, S.A., Morbidelli, A., Raymond, S.N., O'Brien, D.P., Walsh, K.J., Rubie, D.C., 2014. Highly siderophile elements in Earth's mantle as a clock for the Moon-forming impact. *Nature* **508**, 84-87.

Jochum, K.P., Weis, U., Schwager, B., Stoll, B., Wilson, S.A., Haug, G.H., Andreae, M.O., Enzweiler, J., 2016. Reference Values Following ISO Guidelines for Frequently Requested Rock Reference Materials. *Geostand. Geoanal. Res.* **40**, 333-350.

Juteau, M., Pagel, M., Michard, A., Albarede, F., 1988. Assimilation of continental crust by komatiites in the Precambrian basement of the Carswell structure (Saskatchewan, Canada). *Contributions to Mineralogy and Petrology* **99**, 219-225.

Kelemen, P.B., Shimizu, N., Salters, V.J.M., 1995. Extraction of Mid-Ocean-Ridge Basalt from the Upwelling Mantle by Focused Flow of Melt in Dunite Channels. *Nature* **375**, 747-753.

Kimura, K., Lewis, R.S., Anders, E., 1974. Distribution of gold and rhenium between nickel-iron and silicate melts: implications for the abundance of siderophile elements on the Earth and Moon. *Geochim. Cosmochim. Acta* **38**, 683-701.

Kleine, T., Munker, C., Mezger, K., Palme, H., 2002. Rapid accretion and early core formation on asteroids and the terrestrial planets from Hf-W chronometry. *Nature* **418**, 952-955.

Komiya, T., Yamamoto, S., Aoki, S., Sawaki, Y., Ishikawa, A., Tashiro, T., Koshida, K., Shimojo, M., Aoki, K., Collerson, K.D., 2015. Geology of the Eoarchean, >3.95 Ga, Nulliak supracrustal rocks in the Saglek Block, northern Labrador, Canada: the oldest geological evidence for plate tectonics. *Tectonophysics* **662**, 40-66.

Kruijer, T.S., Kleine, T., Fischer-Goedde, M., Sprung, P., 2015. Lunar tungsten isotopic evidence for the late veneer. *Nature* **520**, 534-+.

Lahaye, Y., Arndt, N., Byerly, G., Chauvel, C., Fourcade, S., Gruau, G., 1995. The influence of alteration on the trace-element and Nd isotopic compositions of komatiites. *Chem. Geol.* **126**, 43-64.

Laurenz, V., Rubie, D.C., Frost, D.J., Vogel, A.K., 2016. The importance of sulfur for the behavior of highly-siderophile elements during Earth's differentiation. *Geochim. Cosmochim. Acta* **194**, 123-138.

Liu, J., Pearson, D.G., 2014. Rapid, precise and accurate Os isotope ratio measurements of nanogram to sub-nanogram amounts using multiple Faraday collectors and amplifiers equipped with 10^{12} Ωresistors by N-TIMS. *Chem. Geol.* **363**, 301-311.

Liu, J., Sharp, M., Ash, R.D., Kring, D.A., Walker, R.J., 2015. Diverse impactors in Apollo 15 and 16 impact melt rocks: evidence from osmium isotopes and highly siderophile elements. *Geochim. Cosmochim. Acta* **155**, 122-153.

Liu, J., Touboul, M., Ishikawa, A., Walker, R.J., Pearson, D.G., 2016. Widespread tungsten isotope anomalies and W mobility in crustal and mantle rocks of the Eoarchean Saglek Block, northern Labrador, Canada: implications for early Earth processes and W recycling. *Earth Planet. Sci. Lett.* **448**, 13-23.

Lorand, J.P., Alard, O., Godard, M., 2009. Platinum-group element signature of the primitive mantle rejuvenated by melt-rock reactions: evidence from Sumail peridotites (Oman Ophiolite). *Terra Nova* **21**, 35-40.

Ludwig, K.R., 2006. Isoplot/Ex version 3.41d: a geochronological toolkit for Microsoft Excel. *Berkeley Geochronology Center: Special Publication No.4*.

Luguet, A., Nowell, G.M., Pearson, D.G., 2008. $^{184}Os/^{188}Os$ and $^{186}Os/^{188}Os$ measurements by Negative Thermal Ionisation Mass Spectrometry (N-TIMS): effects of interfering

element and mass fractionation corrections on data accuracy and precision. *Chem. Geol.* **248**, 342-362.

Luguet, A., Behrens, M., Pearson, D.G., Konig, S., Herwartz, D., 2015. Significance of the whole rock Re-Os ages in cryptically and modally metasomatised cratonic peridotites: Constraints from HSE-Se-Te systematics. *Geochim. Cosmochim. Acta* **164**, 441-463.

Maier, W.D., Barnes, S.J., Campbell, I.H., Fiorentini, M.L., Peltonen, P., Smithies, R.H., 2009. Progressive mixing of meteoritic veneer into the early Earth's deep mantle. *Nature* **460**, 620-623.

Malvoisin, B., 2015. Mass transfer in the oceanic lithosphere: Serpentinization is not isochemical. *Earth Planet. Sci. Lett.* **430**, 75-85.

Mann, U., Frost, D.J., Rubie, D.C., Becker, H., Audétat, A., 2012. Partitioning of Ru, Rh, Pd, Re, Ir and Pt between liquid metal and silicate at high pressures and high temperatures - implications for the origin of highly siderophile element concentrations in the Earth's mantle. *Geochim. Cosmochim. Acta* **84**, 593-613.

McDonough, W.F., Sun, S.-S., 1995. The composition of the Earth. *Chem. Geol.* **120**, 223-253.

McGregor, V.R., 1973. The early Precambrian gneisses of the Godthaab district, West Greenland. *Phil. Trans. R. Soc. Lond.* **A273**, 343-358.

Meisel, T., Walker, R.J., Irving, A.J., Lorand, J.-P., 2001. Osmium isotopic compositions of mantle xenoliths: a global perspective. *Geochim. Cosmochim. Acta* **65**, 1311-1323.

Morino, P., Caro, G., Reisberg, L., Schumacher, A., 2017. Chemical stratification in the post-magma ocean Earth inferred from coupled 146,147Sm–142,143Nd systematics in ultramafic rocks of the Saglek block (3.25–3.9 Ga; northern Labrador, Canada). *Earth Planet. Sci. Lett.* **463**, 136-150.

Mundl, A., Touboul, M., Jackson, M.G., Day, J.M.D., Kurz, M.D., Lekic, V., Helz, R.T., Walker, R.J., 2017. Tungsten-182 heterogeneity in modern ocean island basalts. *Science* **356**, 66-+.

Mungall, J.E., Brenan, J.M., 2014. Partitioning of platinum-group elements and Au between sulfide liquid and basalt and the origins of mantle-crust fractionation of the chalcophile elements. *Geochim. Cosmochim. Acta* **125**, 265-289.

Norman, M.D., Borg, L.E., Nyquist, L.E., Bogard, D.D., 2003. Chronology, geochemistry, and petrology of a ferroan noritic anorthosite clast from Descartes breccia 67215: Clues to the age, origin, structure, and impact history of the lunar crust. *Meteoritics & Planetary Science* **38**, 645-661.

Nutman, A.P., Collerson, K.D., 1991. Very early Archean crustal-accreion complexes preserved in the North Atlantic craton. *Geology* **19**, 791-794.

Nutman, A.P., McGregor, V.R., Friend, C.R.L., Bennett, V.C., Kinney, P.D., 1996. The Itsaq Gneiss Complex of southern West Greenland; the world's most extensive record of early crustal evolution (3900–3600 Ma). *Precamb. Res.* **78**, 1–39.

Pearson, D.G., Irvine, G.J., Ionov, D.A., Boyd, F.R., Dreibus, G.E., 2004. Re–Os isotope systematics and platinum group element fractionation during mantle melt extraction: a study of massif and xenolith peridotite suites. *Chem. Geol.* **208**, 29-54.

Puchtel, I.S., Humayun, M., 2001. Platinum group element fractionation in a komatiitic basalt lava lake. *Geochim. Cosmochim. Acta* **65**, 2979-2993.

Puchtel, I.S., Humayun, M., Campbell, A.J., Sproule, R.A., Lesher, C.M., 2004. Platinum group element geochemistry of komatiites from the Alexo and Pyke Hill areas, Ontario, Canada. *Geochim. Cosmochim. Acta* **68**, 1361-1383.

Puchtel, I.S., Humayun, M., 2005. Highly siderophile element geochemistry of ^{187}Os-enriched 2.8 Ga Kostomuksha komatiites, Baltic Shield. *Geochim. Cosmochim. Acta* **69**, 1607-1618.

Puchtel, I.S., Humayun, M., Walker, R.J., 2007. Os–Pb–Nd isotope and highly siderophile and lithophile trace element systematics of komatiitic rocks from the Volotsk suite, SE Baltic Shield. *Precamb. Res.* **158**, 119-137.

Puchtel, I.S., Walker, R.J., James, O.B., Kring, D.A., 2008. Osmium isotope and highly siderophile element systematics of lunar impact melt breccias: implications for the late accretion history of the Moon and Earth. *Geochim. Cosmochim. Acta* **72**, 3022-3042.

Puchtel, I.S., Walker, R.J., Anhaeusser, C.R., Gruau, G., 2009a. Re–Os isotope systematics and HSE abundances of the 3.5 Ga Schapenburg komatiites, South Africa: hydrous melting or prolonged survival of primordial heterogeneities in the mantle? *Chem. Geol.* **262**, 355-369.

Puchtel, I.S., Walker, R.J., Brandon, A.D., Nisbet, E., 2009b. Pt–Re–Os and Sm–Nd isotope and HSE and REE systematics of the 2.7 Ga Belingwe and Abitibi komatiites. *Geochim. Cosmochim. Acta* **73**, 6367-6389.

Puchtel, I.S., Walker, R.J., Touboul, M., Nisbet, E.G., Byerly, G.R., 2014. Insights into early Earth from the Pt-Re-Os isotope and highly siderophile element abundance systematics of Barberton komatiites. *Geochim. Cosmochim. Acta* **125**, 394-413.

Puchtel, I.S., Blichert-Toft, J., Touboul, M., Horan, M.F., Walker, R.J., 2016a. The coupled ^{182}W-^{142}Nd record of early terrestrial mantle differentiation. *Geochem. Geophys. Geosyst.* **17**, 2168-2193.

Puchtel, I.S., Touboul, M., Blichert-Toft, J., Walker, R.J., Brandon, A.D., Nicklas, R.W., Kulikov, V.S., Samsonov, A.V., 2016b. Lithophile and siderophile element systematics of Earth's mantle at the Archean–Proterozoic boundary: evidence from 2.4 Ga komatiites. *Geochim. Cosmochim. Acta* **180**, 227-255.

Rehkämper, M., Halliday, A.N., Alt, J., Fitton, J.G., Zipfel, J., Takazawa, E., 1999. Non-chondritic platinum-group element ratios in oceanic mantle lithosphere: petrogenetic signature of melt percolation? *Earth Planet. Sci. Lett.* **172**, 65-81.

Riches, A.J.V., Day, J.M.D., Walker, R.J., Simonetti, A., Liu, Y., Neal, C.R., Taylor, L.A., 2012. Rhenium–osmium isotope and highly-siderophile-element abundance systematics of angrite meteorites. *Earth Planet. Sci. Lett.* **353–354**, 208-218.

Righter, K., Campbell, A.J., Humayun, M., Hervig, R.L., 2004. Partitioning of Ru, Rh, Pd, Re, Ir, and Au between Cr-bearing spinel, olivine, pyroxene and silicate melts. *Geochim. Cosmochim. Acta* **68**, 867-880.

Rizo, H., Walker, R.J., Carlson, R.W., Horan, M.F., Mukhopadhyay, S., Manthos, V., Francis, D., Jackson, M.G., 2016a. Preservation of Earth-forming events in the tungsten isotopic composition of modern flood basalts. *Science* **352**, 809-812.

Rizo, H., Walker, R.J., Carlson, R.W., Touboul, M., Horan, M.F., Puchtel, I.S., Boyet, M., Rosing, M.T., 2016b. Early Earth differentiation investigated through ^{142}Nd, ^{182}W, and highly siderophile element abundances in samples from Isua, Greenland. *Geochim. Cosmochim. Acta* **175**, 319-336.

Robin-Popieul, C.C.M., Arndt, N.T., Chauvel, C., Byerly, G.R., Sobolev, A.V., Wilson, A., 2012. A New Model for Barberton Komatiites: Deep Critical Melting with High Melt Retention. *J. Petrol.* **53**, 2191-2229.

Rollinson, H., Appel, P.W.U., Frei, R., 2002. A metamorphosed, early Archaean chromitite from west Greenland: implications for the genesis of Archaean anorthositic chromitites. *J. Petrol.* **43**, 2143-2170.

Rollinson, H., 2007. Recognising early Archaean mantle: a reappraisal. *Contributions to Mineralogy and Petrology* **154**, 241-252.

Ryan, B., Martineau, Y., 2012. Revised and coloured edition of 1992 map showing the Geology of the Saglek Fiord-Hebron Fiord area, Labrador (NTS 14L/2, 3, 6, 7).

Government of Newfoundland and Labrador, Department of Natural Resources, Geological Survey, Map 2012-15, p. Open File 14L0091.

Schiøtte, L., Bridgwater, D., Collerson, K.D., Nutman, A.P., Ryan, A.B., 1986. Chemical and isotopic effects of late Archaean high-grade metamorphism and granite injection on early Archaean gneisses, Saglek-Hebron, northern Labrador, in: Dawson, J.B., Carswell, D.A., Hall, J., Wedepohl, H.H. (Eds.), The Nature of the Lower Continental Crust, Geol. Soc., Spec. Publ., pp. 261–273.

Schiøtte, L., Compston, W., Bridgwater, D., 1989a. Ion probe U-Th-Pb zircon dating of polymetamorphic orthogneisses from northern Labrador, Canada. *Canadian Journal of Earth Science* **26**, 1533-1556.

Schiøtte, L., Compston, W., Bridgwater, D., 1989b. U-Th-Pb ages of single zircons in Archaean supracrustals from Nain Province, Labrador, Canada. *Canadian Journal of Earth Science* **26**, 2636-2644.

Schoenberg, R., Kamber, B.S., Collerson, K.D., Moorbath, S., 2002. Tungsten isotope evidence from ~3.8-Gyr metamorphosed sediments for early meteorite bombardment of the Earth. *Nature* **418**, 403-405.

Senda, R., Ishikawa, A., 2014. Osmium in reagents and environment: implication for measurements of low level Os and identification of the sources of Os blanks. *JAMSTEC Rep. Res. Dev.* **18**, 17-28. (in Japanese with English abstract).

Sharp, M., Gerasimenko, I., Loudin, L.C., Liu, J.G., James, O.B., Puchtel, I.S., Walker, R.J., 2014. Characterization of the dominant impactor signature for Apollo 17 impact melt rocks. *Geochim. Cosmochim. Acta* **131**, 62-80.

Shimojo, M., Yamamoto, S., Sakata, S., Yokoyama, T.D., Maki, K., Sawaki, Y., Ishikawa, A., Aoki, K., Aoki, S., Koshida, K., Tashiro, T., Hirata, T., Collerson, K.D., Komiya, T., 2016. Occurrence and geochronology of the Eoarchean, similar to 3.9 Ga, Iqaluk Gneiss in the Saglek Block, northern Labrador, Canada: evidence for the oldest supracrustal rocks in the world. *Precamb. Res.* **278**, 218-243.

Shirey, S.B., Walker, R.J., 1998. The Re–Os isotope system in cosmochemistry and high-temperature geochemistry. *Annual Reviews of Earth and Planetary Sciences* **26**, 423-500.

Smoliar, M.I., Walker, R.J., Morgan, J.W., 1996. Re-Os ages of group IIA, IIIA, IVA, and IVB iron meteorites. *Science* **271**, 1099-1102.

Streckeisen, A., 1976. To each plutonic rock its proper name. *Earth-Science Reviews* **12**, 1-33.

Szilas, K., Kelemen, P.B., Rosing, M.T., 2015. The petrogenesis of ultramafic rocks in the >3.7 Ga Isua supracrustal belt, southern West Greenland: geochemical evidence for two distinct magmatic cumulate trends. *Gondwana Research* **28**, 565-580.

Tera, F., Papanastassiou, D.A., Wasserburg, G.J., 1974. Isotopic evidence for a terminal lunar cataclysm. *Earth Planet. Sci. Lett.* **22**, 1-21.

Touboul, M., Puchtel, I.S., Walker, R.J., 2012. ^{182}W evidence for long-term preservation of early mantle differentiation products. *Science* **335**, 1065-1069.

Touboul, M., Liu, J., O'Neil, J., Puchtel, I.S., Walker, R.J., 2014. New insights into the Hadean mantle revealed by ^{182}W and highly siderophile element abundances of supracrustal rocks from the Nuvvuagittuq Greenstone Belt, Quebec, Canada. *Chem. Geol.* **383**, 63-75.

Touboul, M., Puchtel, I.S., Walker, R.J., 2015. Tungsten isotopic evidence for disproportional late accretion to the Earth and Moon. *Nature* **520**, 530-+.

van Acken, D., Brandon, A.D., Lapen, T.J., 2012. Highly siderophile element and osmium isotope evidence for postcore formation magmatic and impact processes on the aubrite parent body. *Meteoritics & Planetary Science* **47**, 1606-1623.

Walker, R.J., Carlson, R.W., Shirey, S.B., Boyd, F.R., 1989. Os, Sr, Nd, and Pb isotope systematics of southern African peridotite xenoliths: implications for the chemical evolution of subcontinental mantle. *Geochim. Cosmochim. Acta* **53**, 1583-1595.

Walker, R.J., Horan, M.F., Morgan, J.W., Becker, H., Grossman, J.N., Rubin, A.E., 2002. Comparative ^{187}Re-^{187}Os systematics of chondrites: implications regarding early solar system processes. *Geochim. Cosmochim. Acta* **66**, 4187-4201.

Walker, R.J., 2009. Highly siderophile elements in the Earth, Moon and Mars: Update and implications for planetary accretion and differentiation. *Chemie der Erde - Geochemistry* **69**, 101-125.

Walter, M.J., 2003. Melt extraction and compositional variability in mantle lithosphere. *The Mantle & Core. Treatise on Geochemistry* **2**, 363–394.

Wendt, J.I., Collerson, K.D., 1999. Early Archaean U/Pb fractionation and timing of late Archaean high-grade metamorphism in the Saglek-Hebron segment of the North Atlantic Craton. *Precamb. Res.* **93**, 281-297.

Willbold, M., Elliott, T., Moorbath, S., 2011. The tungsten isotopic composition of the Earth's mantle before the terminal bombardment. *Nature* **477**, 195-198.

Willbold, M., Mojzsis, S.J., Chen, H.W., Elliott, T., 2015. Tungsten isotope composition of the Acasta Gneiss Complex. *Earth Planet. Sci. Lett.* **419**, 168-177.

Wittig, N., Webb, M., Pearson, D.G., Dale, C.W., Ottley, C.J., Hutchison, M., Jensen, S.M., Luguet, A., 2010. Formation of the North Atlantic Craton: timing and mechanisms constrained from Re-Os isotope and PGE data of peridotite xenoliths from SW Greenland. *Chem. Geol.* **276**, 166-187.

Yin, Q., Jacobsen, S.B., Yamashita, K., Blichert-Toft, J., Telouk, P., Albarede, F., 2002. A short timescale for terrestrial planet formation from Hf-W chronometry of meteorites. *Nature* **418**, 949-952.

FIGURE CAPTIONS

Figure 1. Geological map of the Saglek-Hebron segment of the North Atlantic Craton in northern Labrador, Canada, simplified after Schiøtte et al. (1986) and Ryan and Martineau (2012) with sample localities. Inset map shows North Atlantic Craton encompassed by a thick dashed line and the Saglek-Hebron area in northern Labrador.

Figure 2. Photomicrographs (left panels: transmitted light, right panels: plane polarised light) of representative samples of Saglek ultramafic suites. (A-B) dunite (KC91-21B) and (C-D) amphibole harzburgite from lithospheric mantle suite (KC87-114K). (E-F) amphibole harzburgite from Cape Uivak layered body (KC91-32A). (D-F) olivine-pyroxene hornblendite from metakomatiite suite (KC87-111F). Peridotitic samples from lithospheric mantle suite are dominated by fine-grained olivine displaying a polygonal texture with minor spinel, orthopyroxene and hydrous phases such amphibole and phlogopite. Well-equilibrated 120˚ grain boundaries may rule out extensive deformation, but they could have been recrystallised under high-temperature conditions.

Figure 3. (A) Covariation of Mg/Si with Al/Si (by weight), (B) CaO versus. MgO, (C) NiO versus MgO and (D) Cr_2O_3 versus MgO for Saglek ultramafic suites. Open and filled

circles are for olivine- and amphibole-rich types of lithospheric mantle suite, respectively. Open and filled diamonds are for a Cape Uivak layered body and metakomatiite suite, respectively. Eoarchean (small filled squares) and Mesoarchean suites (small open circles) of Saglek ultramafic rocks studied by Morino et al. (2017), model compositions of primitive upper mantle (stars; Walter, 2003 and references therein), compilations of abyssal and ophiolite peridotites (field encompased by thick gray line; Malvoisin, 2015 and references therein) and Archean komatiites (small filled diamonds in grey field; Robin-Popieul et al., 2012; Puchtel et al., 2016a and references therein) are also shown for comparison. All data are recalculated on an anhydrous basis.

Figure 4. Chondrite-normalised REE patterns and primitive mantle-normalised trace element diagrams for olivine-rich types (mainly dunites) of lithospheric mantle suites and metakomatiites (A and C) and amphibole-rich type (amphibole harzburgite to hornblendite) of lithospheric mantle suites plus the Cape Uivak layered body (B and D). Symbols are the same as Fig. 3. Eoarchean (in A and C) and Mesoarchean suites (in B and D) of Saglek ultramafic rocks studied by Morino et al. (2017) are shown for comparisons (shaded fields). Chondrite and primitive mantle values are from Anders and Grevesse (1989) and McDonough and Sun (1995), respectively.

Figure 5. Highly siderophile element patterns for Saglek ultramafic suites. CI chondrite normalising values are from Fischer-Gödde et al. (2010). (A) olivine-rich lithospheric mantle suite compared with less modified peridotite xenoliths from southwest Greenland in North Atlantic Craton (shaded field: Wittig et al., 2010). (B) amphibole-rich type of lithospheric mantle suite compared with modern lherzolites with Al_2O_3 contents >2.0 wt.% (dark shaded field: Pearson et al., 2004; Becker et al., 2006; Fischer-Gödde et al., 2011) and metaperidotites from Isua supracrustal belt and adjacent ~3.8 Ga orthogneiss terrain, southwest Greenland (shaded field: Rizo et al., 2016b; Dale et al., 2017). (C) Layered-type of lithospheric mantle suite (Cape Uivak layered body) are compared with ~3.8 Ga Ujaragssuit nunât metaperidotites from southwest Greenland (shaded field: Coggon et al., 2015). (D) olivine and/or pyroxene-bearing hornblendites from metakomatiite suite, compared with calculated compositions of emplaced komatiite lava (shaded field: Puchtel et al., 2014 and references therein).

Figure 6. Ru versus Cr_2O_3 for all analysed samples from Saglek ultramafic suites. Symbols are the same as Fig. 3. Linear regression line is calculated for data points of Cape Uivak layered body (excluding two samples of hornblendites showing low Ru and Cr_2O_3 contents.

Figure 7. Measured $^{187}Re/^{188}Os$ versus $^{187}Os/^{188}Os$ for Saglek ultramafic suites. Panel B shows the expanded portion of panel A featuring samples having unradiogenic $^{187}Os/^{188}Os$ ratios. Series of reference isochrons shown in both panels are for samples formed from a parental reservoir with the average chondritic isotopic composition (including carbonaceous, enstatite, and ordinary chondrites), and were calculated using the ^{187}Re decay constant $\lambda = 1.666 \times 10^{-11}$ year^{-1} (Smoliar et al., 1996; Shirey and Walker, 1998; Walker et al., 2002), an early Solar System initial $^{187}Os/^{188}Os = 0.09531$ at T = 4558 Ma, and $^{187}Re/^{188}Os = 0.40186$. Background data in both panels are whole-rock data of Eoarchean mafic-ultramafic rocks from Ujaragssuit nunât, southwest Greenland (Bennett et al., 2002; Rollinson et al., 2002; Coggon et al., 2015), Isua supracrustal belt and adjacent orthogneiss, southwest Greenland (Frei and Jensen, 2003; Frei et al., 2004; Rizo et al., 2016b; Dale et al., 2017) and Nuvvuagittuq greenstone belt, Canada (Touboul et al., 2015). Unradiogenic groups of lithospheric mantle and metakomatiite suites yield Re-depletion model ages (T_{RD}) of 2.8-3.3 Ga and 3.4-3.6 Ga, respectively. Panel (C) and (D) display regression lines calculated with Isoplot (version 3.41d, Ludwig, 2006) for selected samples of metakomatiite and amphibole-rich type of lithospheric mantle suites, respectively (see text for details).

Figure 8. (A) Pd/Ir versus Al_2O_3, (B) Pt/Ir versus Al_2O_3, (C) Ru/Ir versus MgO and (D) Ru versus MgO for dunites and metakomatiites from the two Saglek ultramafic suites. Linear regression lines in (A) and (B) were calculated for each rock types (excluding high-Al_2O_3 samples for metakomatiites). Model compositions of primitive upper mantle (stars) and chondritic ratios (dotted lines) are from Becker et al. (2006) and Fischer-Gödde et al. (2010), respectively. In panel (C) and (D), three data points of ~3.8 Ga Isua ultramafics possessing mantle-like HSE patterns and MgO contents are also shown for comparisons (Dale et al., 2017). Background data in (D) are for Archean komatiites (small filled diamonds) and less modified peridotite xenoliths from southwest Greenland in North Atlantic Craton (small open circles). Data sources for komatiites are as in Figure 5.

Figure 9. (A) Initial $^{187}Os/^{188}Os$ isotopic compositions of the Archean komatiite systems (filled circles), Saglek metakomatiites and lithospheric mantle suites (filled diamond and open circle, respectively) and of Isua boninitic basalts (open diamond) plotted as function of age determined by isochron methods. For Eoarchean ultramafic rocks of southwest Greenland (Isua supracrustal belt, and Ujaragssuit nunât area) and Nuvvuagittuq greenstone belt, the lowest present-day $^{187}Os/^{188}Os$ from each locality and sample type are

plotted as function of age. Possible range of initial $^{187}Os/^{188}Os$ of lithospheric mantle (grey field) and metakomatiite suites (dark grey field) of unradiogenic Saglek ultramafic rocks are also estimated by assuming that the measured $^{187}Re/^{188}Os$ ratios represent those of their initial formation. Upper limits of age for the lithospheric mantle and metakomatiite suites were set to 3365 + 100 Ma and 3782 + 93 Ma, respectively, derived from ^{147}Sm-^{143}Nd dates (Morino et al., 2017), whereas lower limits were derived from intersection of evolution trajectories for each sample of $^{187}Re/^{188}Os$ with the chondritic evolution line. Dotted line indicates the evolution trajectory of PUM (Meisel et al., 2001). Panel (B) displays the estimated Ru abundances in the sources of lithospheric mantle and metakomatiite suites of the Saglek ultramafic rocks compared with those for Archean komatiites. Open circle and filled diamond represent our estimates on the sources of Saglek lithospheric mantle and metakomatiite suites based on their whole rock Re-Os errorchrons and average Ru abundance (±1 sigma) of high-Mg samples (MgO >25 wt.%). Possible range of Ru in sources for lithospheric mantle (grey field) and metakomatiite suites (dark grey field) are also indicated. The data sources for Archean-Early Proterozoic komatiites and mafic-ultramafic rocks from southwest Greenland and Nuvvuagittuq are same as in Figures 5, 7 and 8.

Table 1: Mineral assemblage and olivine-spinel compositions of Saglek ultramafic rocks from Northern Labrador, North Atlantic Craton

Table 1 footnote: Ol, olivine; Sp, spinel; Opx, orthopyroxene; Amp, amphibole; Phl, phlogopite; Chl, chlorite; Fo, forsterite content =100 Mg/(Mg+Fe); Mg# in spinel = 100 $Mg/(Mg+Fe^{2+})$, Cr# in spinel = 100 Cr/(Cr+Al); open circle, present; filled circle, psuedomorphs or altered products are present; horizontal bar, absent.

Table 2: Whole rock major element compositions of Saglek ultramafic rocks from Northern Labrador, North Atlantic Craton

Table 2 footnote: Concentration values presented are in wt.%. LOl, loss on ignition. RV. Reference values of MRG-1 and JP-1 are from Govindaraju (1994) and Imai et al. (1995), respectively

Table 3: Whole rock trace element compositions of selected Saglek ultramafic rocks from Northern Labrador, North Atlantic Craton

Table 3 footnote: Concentration values presented are in mg/g except for Ti, Cr and Ni in g/100 g. Concentration of W are from Liu et al. (2016). Reference values (RV) and information values (IV in italics) are from Jochum et al. (2016).

Table 4: HSE concentrations and Re-Os isotopes data of Saglek ultramafic rocks from Northern Labrador, North Atlantic Craton

Table 4 footnote: Analyses recalculated on an anhydrous basis; dupl., duplicate analyses; $^{187}Os/^{188}Os$ ratios normalised using $^{192}Os/^{188}Os = 3.08271$ and corrected using $^{18}O/^{16}O$ and $^{17}O/^{16}O$ of 0.002045 and 0.000371 respectively; Uncertainties on $^{187}Re/^{188}Os$ and $^{187}Os/^{188}Os$ (given in brackets, refer to least significant digits) are estimated by error propagation of isotope measurements (2SE) and blank correction. T_{RD} and T_{MA} ages (Ga) are calculated by using ^{187}Re decay constant $\lambda_{Re} = 1.666 \times 10^{-11}$ year^{-1} relative to the evolution of average chondrite with initial $^{187}Os/^{188}Os = 0.09531$ at 4.558 Ga, and $^{187}Re/^{188}Os = 0.40186$ (Smoliar et al., 1996; Shirey and Walker, 1998). Initial $^{187}Os/^{188}Os$ ratios are recalculated by using age values of Sm-Nd isochrons, which are 3.362 Ga for lithospheric mantle suite including Cape Uivak layered body, and 3.782 Ga for metakomatiite suite, respectively (Morino et al., 2017). Unrealistic values of model ages and initial $^{187}Os/^{188}Os$ ratios are not presented. Full data and compilation of published values for UB-N and JP-1 are in Ishikawa et al. (2014).

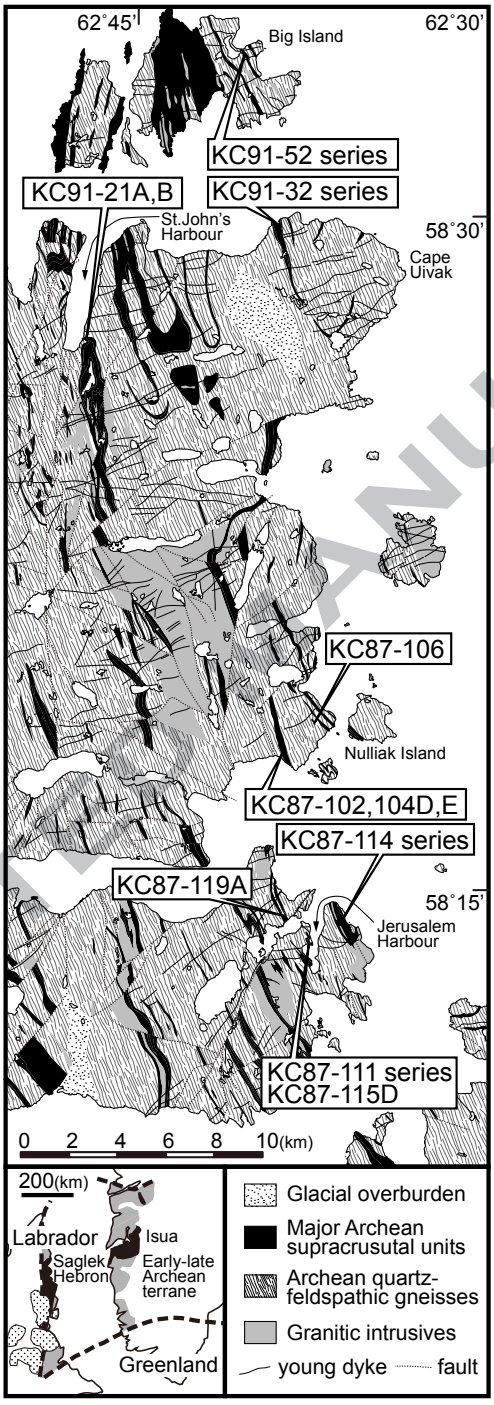

Fig. 1 Ishikawa et al. (submitted to *HSE special volume on GCA*)

Figure2

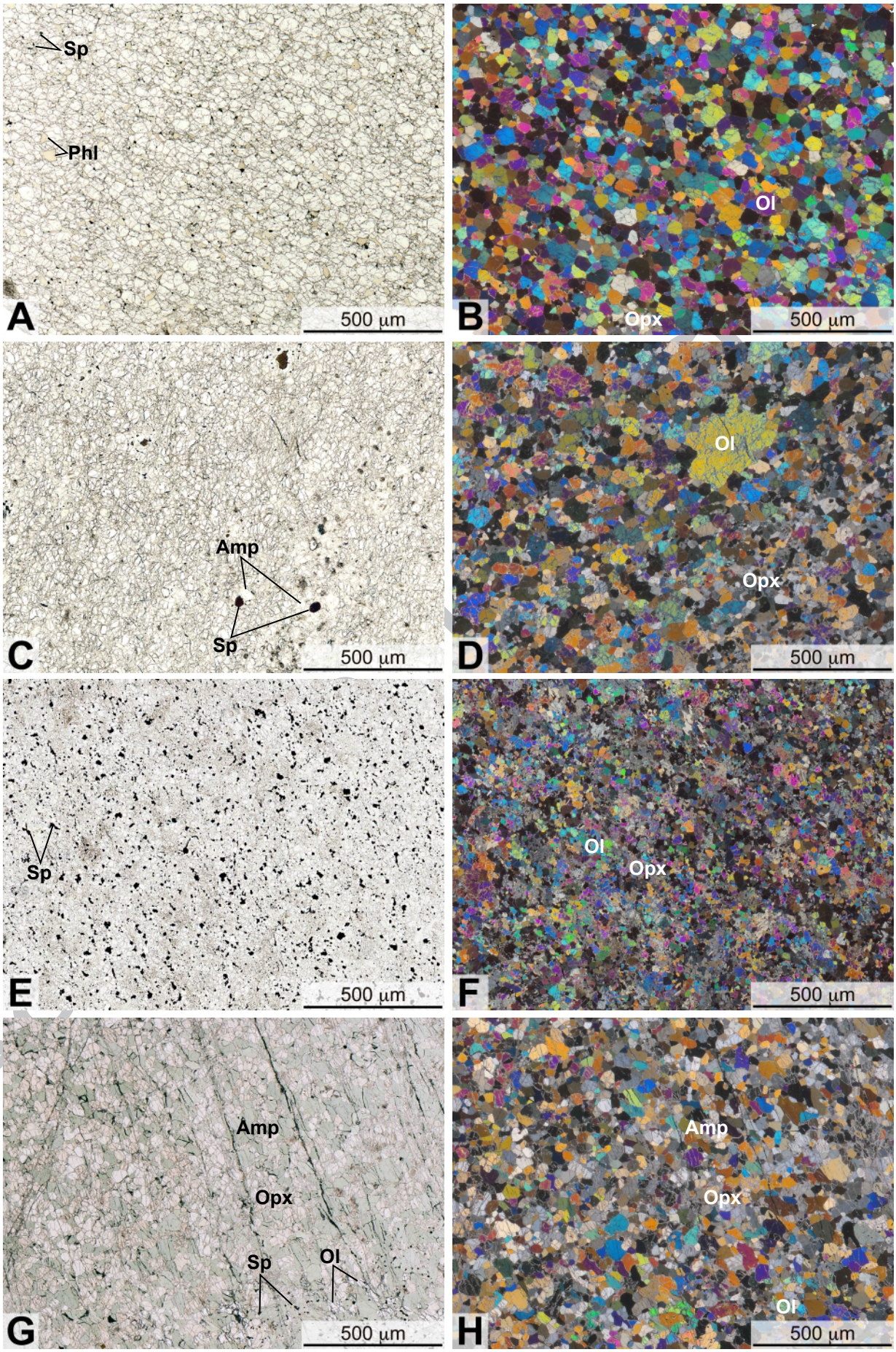

Fig. 2 Ishikawa et al. (submitted to *HSE special volume on GCA*)

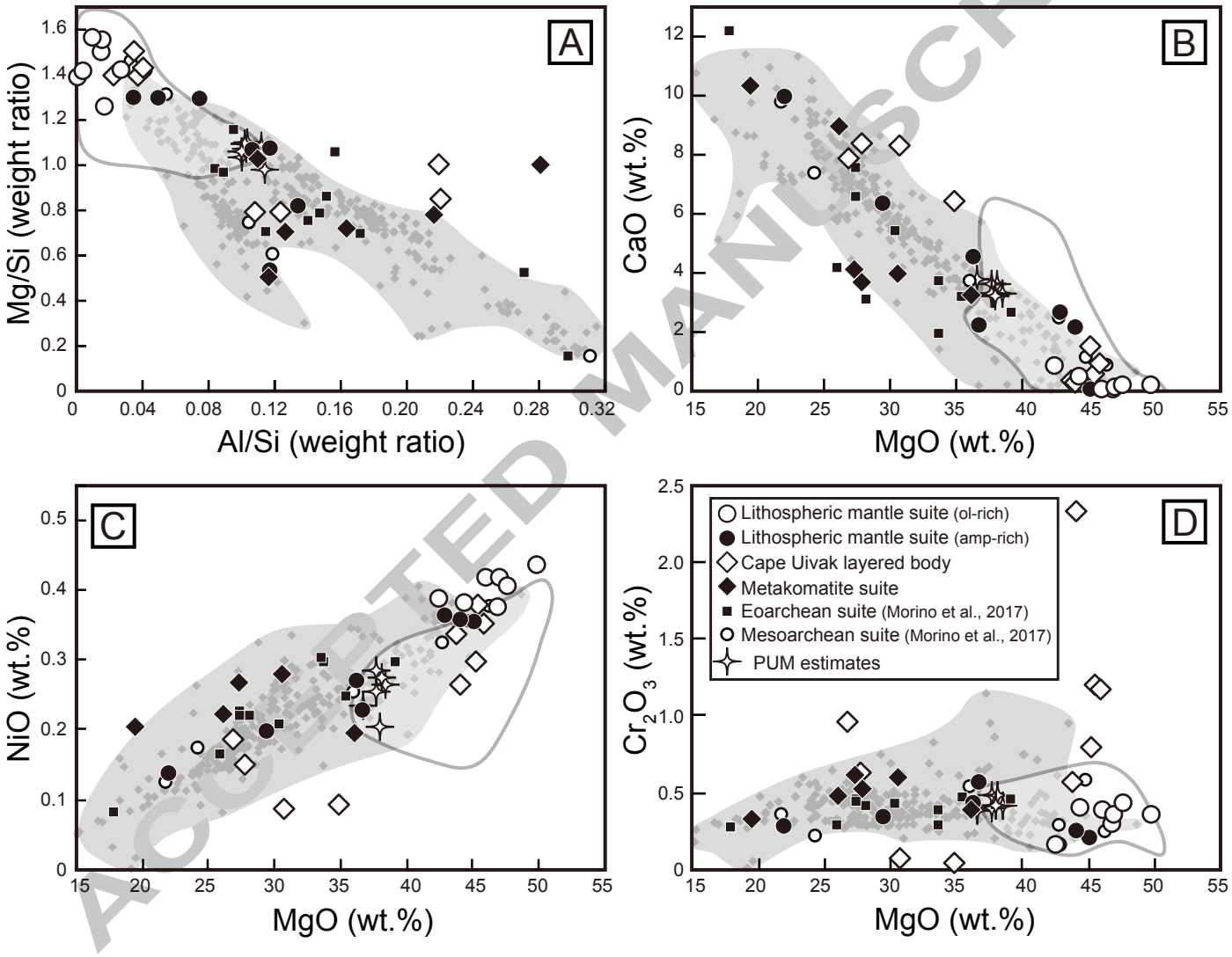

Fig. 3 Ishikawa et al. (submitted to *HSE special volume on GCA*)

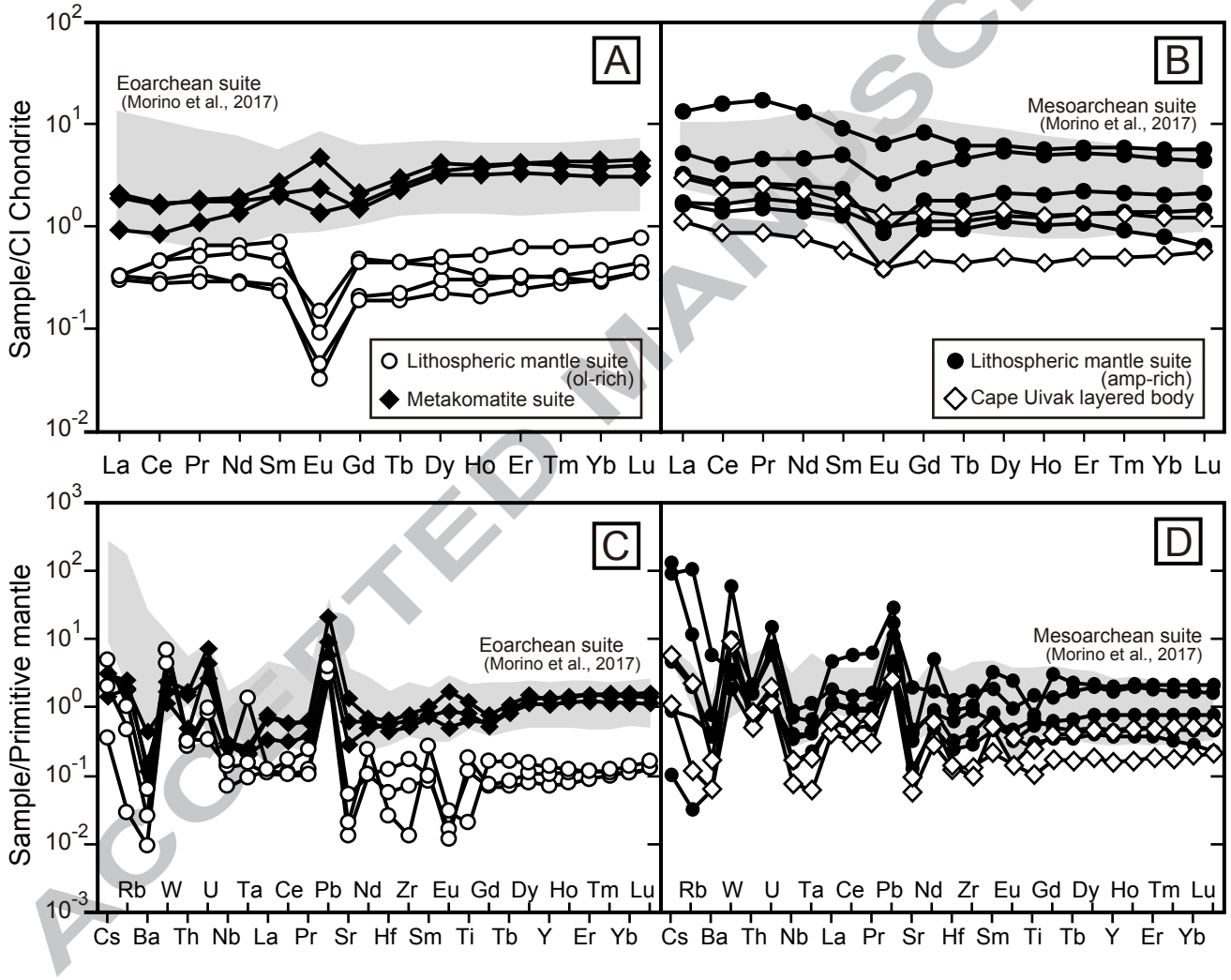

Fig. 4 Ishikawa et al. (submitted to *HSE special volume on GCA*)

Figure5

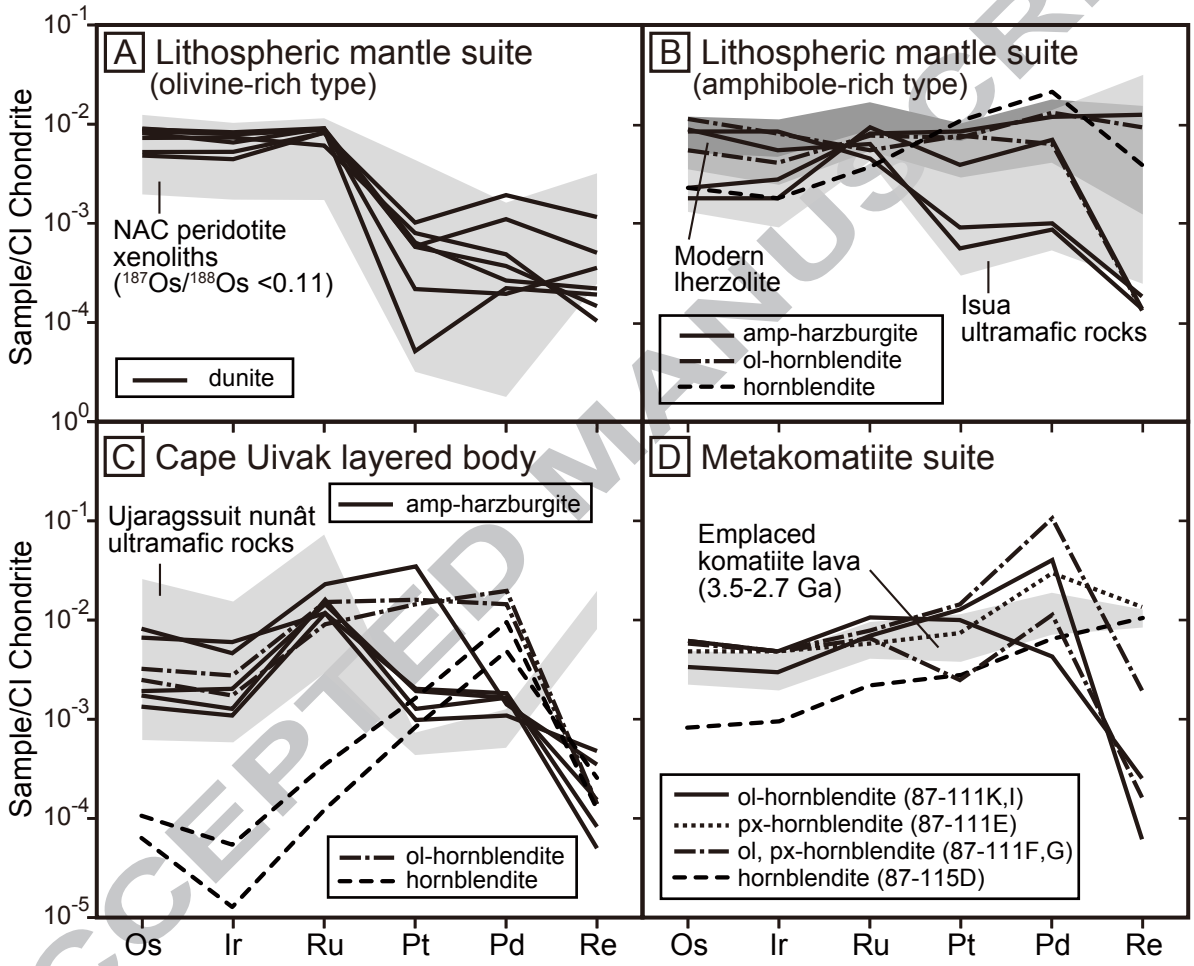

Fig. 5 Ishikawa et al. (submitted to *HSE special volume on GCA*)

Figure6

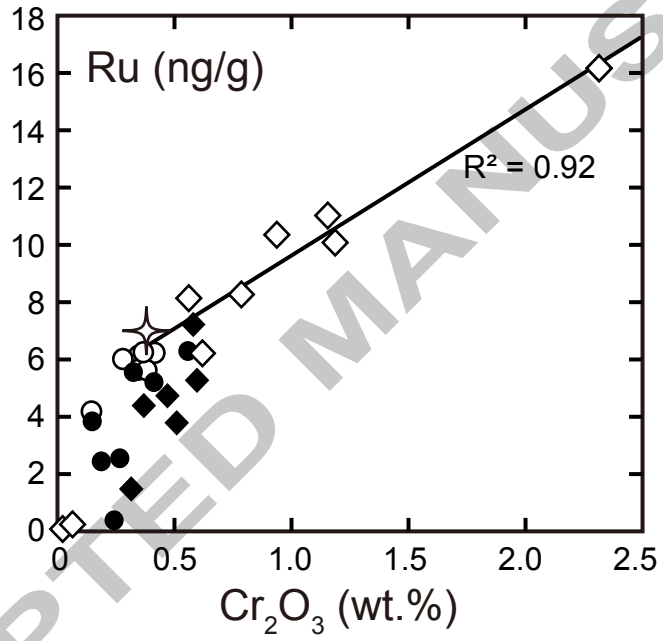

Fig. 6 Ishikawa et al. (submitted to *HSE special volume on GCA*)

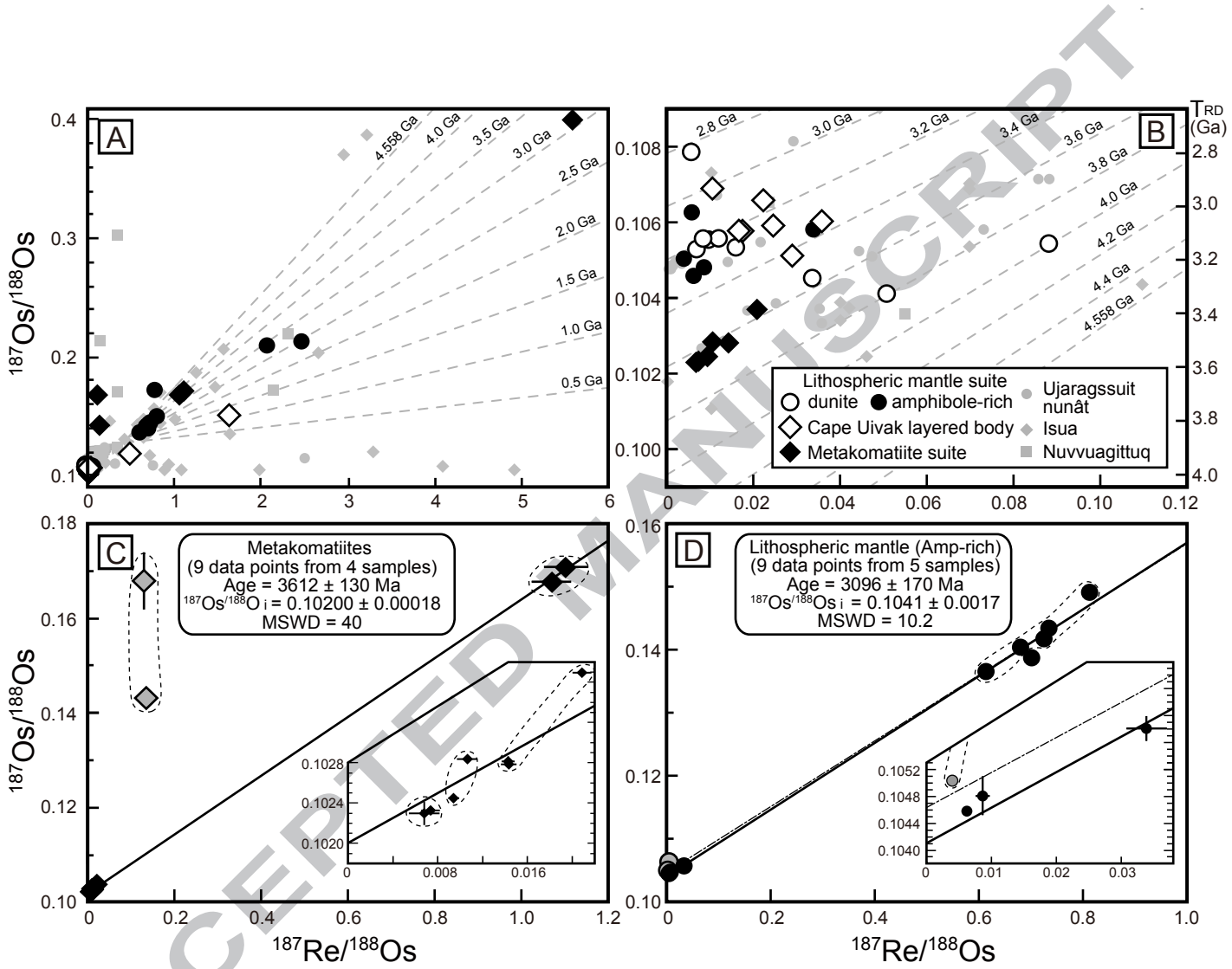

Fig. 7 Ishikawa et al. (submitted to *HSE special volume on GCA*)

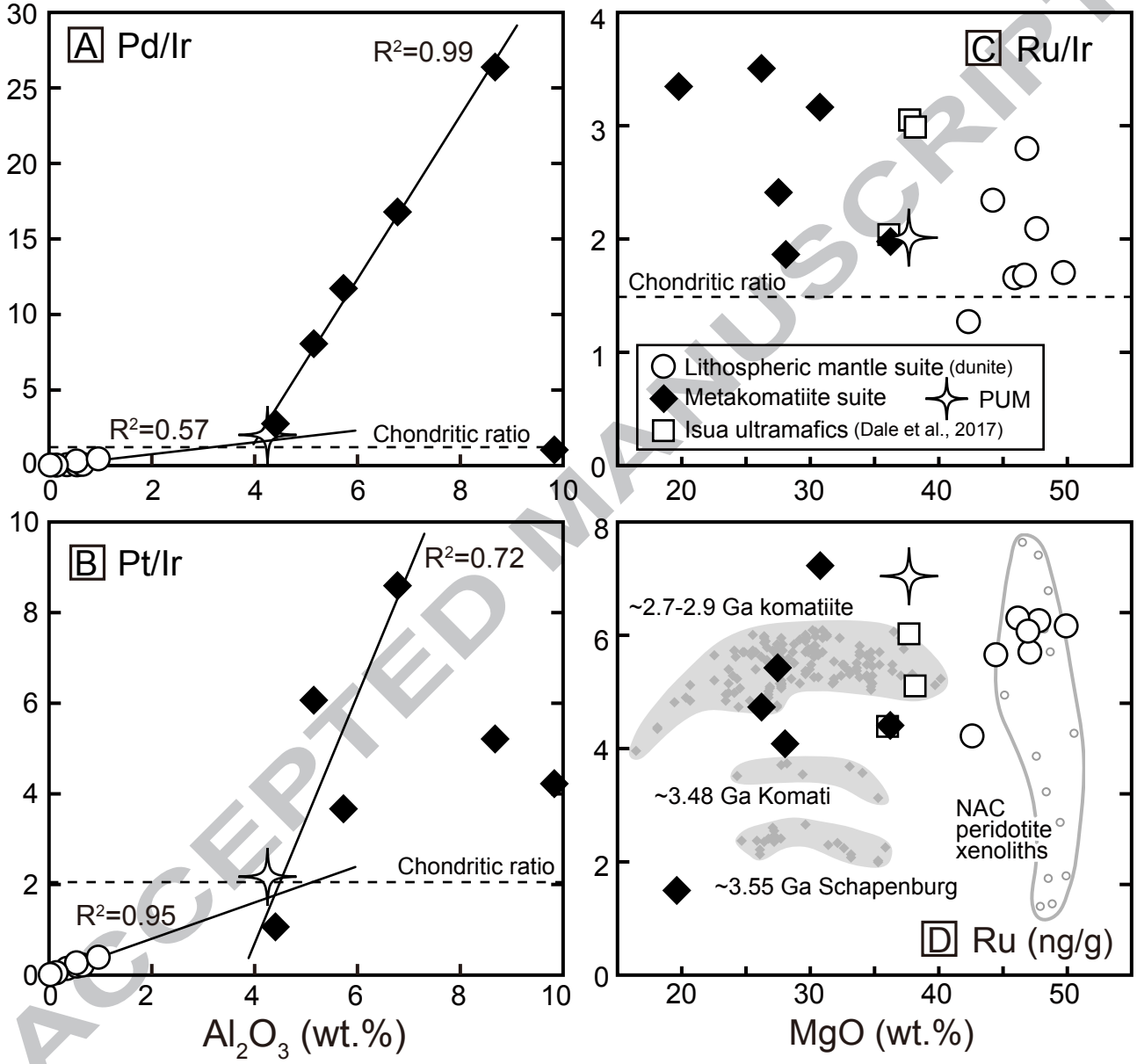

Fig. 8 Ishikawa et al. (submitted to *HSE special volume on GCA*)

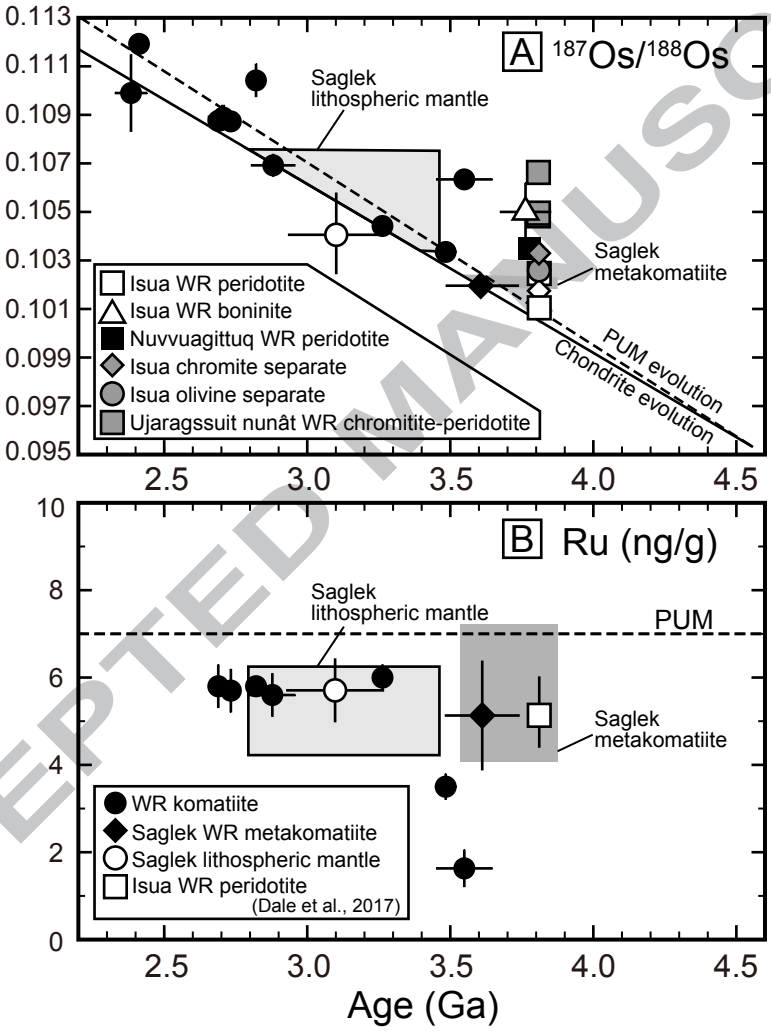

Fig. 9 Ishikawa et al. (submitted to *HSE special volume on GCA*)

Table1

Table 1: Mineral assemblage and olivine-spinel compositions of Saglek ultramafic rocks from Northern Labrador, North Atlantic

Sample	Locality	Rock type	Ol	Sp	Opx	Amp	Phl	Chl	Fo olivine	Mg# spinel	Cr# spinel
Lithospheric mantle suite											
KC87-104D	Nulliak opposite shore	Dunite	●	●	-	-	-	-			
KC87-104E	Nulliak opposite shore	Dunite	○	●	-	-	○	-	91.2	18.1	86.2
KC91-21A	St. Jones Harbor	Dunite	○	●	-	-	○	○	86.8	2.8	96.6
KC91-21B	St. Jones Harbor	Dunite	○	●	○	-	○	-	89.4	13.0	80.8
KC91-52A	Big Island	Dunite	●	●	-	-	-	-			
KC91-52B	Big Island	Dunite	○	●	-	-	-	○	92.2	4.4	95.8
KC91-52D	Big Island	Dunite	○	●	-	-	-	-	92.4	34.1	52.3
KC87-114G	Hebron	Amphibole harzburgite	●	●	-	○	-	-			
KC87-114I	Hebron	Amphibole harzburgite	○	○	-	○	-	-	91.7	53.9	36.3
KC87-114K	Hebron	Amphibole harzburgite	○	○	○	○	-	-	91.1	71.1	15.7
KC87-119A	Hebron	Amphibole harzburgite	○	○	○	○	-	-	87.0	54.2	16.4
KC87-102	Nulliak opposite shore	Olivine hornblendite	●	●	-	○	-	-			
KC91-52C	Big Island	Olivine hornblendite	○	○	-	○	-	○			
KC87-106A	Nulliak opposite shore	Hornblendite	-	-	-	○	○	-			
Cape Uivak layered body											
KC91-32A	Cape Uivak	Amphibole harzburgite	○	●	○	○	-	○	96.6	6.8	92.0
KC91-32B	Cape Uivak	Amphibole harzburgite	○	●	○	○	-	○	96.9	3.9	93.2
KC91-32D	Cape Uivak	Amphibole harzburgite	○	●	○	○	-	○	96.7	3.7	93.0
KC91-32E	Cape Uivak	Amphibole harzburgite	○	●	○	○	-	○	96.3	1.6	98.5
KC91-32F	Cape Uivak	Amphibole harzburgite	○	●	○	○	-	○	96.5	4.2	96.1
KC91-32C-1	Cape Uivak	Olivine hornblendite	○	●	-	○	-	○	96.2	1.4	100.0
KC91-32C-2	Cape Uivak	Hornblendite	○	●	-	○	-	○			
KC91-32C-3	Cape Uivak	Olivine hornblendite	○	●	-	○	-	○			
KC91-32C-4	Cape Uivak	Hornblendite	○	●	-	○	-	○			
Metakomatiite suite											
KC87-111E	Jerusalem Harbor	Pyroxene hornblendite	-	-	○	○	○	-			
KC87-111F	Jerusalem Harbor	Olivine-pyroxene hornblendi	○	○	○	○	-	-	81.9	43.6	12.7
KC87-111G	Jerusalem Harbor	Olivine-pyroxene hornblendi	○	○	○	○	-	-	87.5	55.9	17.8
KC87-111I	Jerusalem Harbor	Olivine hornblendite	●	●	-	○	-	○			
KC87-111K	Jerusalem Harbor	Olivine hornblendite	○	●	-	○	-	-	82.1	16.3	39.6
KC87-115D	Jerusalem Harbor	Hornblendite	-	-	-	○	○	-			

Ol, olivine; Sp, spinel; Opx, orthopyroxene; Amp, amphibole; Phl, phlogopite; Chl, chlorite; Fo, forsterite content =100 Mg/(Mg+Fe); Mg# in spinel = 100 Mg/(Mg+Fe^{2+}), Cr# in spinel = 100 Cr/(Cr+Al); open circle, present; filled circle, psuedomorphs or altered products are

Table2

Table 2: Whole rock major element compositions of Saglek ultramafic rocks from Northern Labrador, North Atlantic Craton

Sample	SiO_2	TiO_2	Al_2O_3	Cr_2O_3	Fe_2O_3	MnO	MgO	NiO	CaO	Na_2O	K_2O	P_2O_5	LOI	Total	Mg/Si	Al/Si	Mg#
Lithospheric mantle suite																	
KC87-104D	36.16	0.007	0.02	0.232	8.03	0.105	38.97	0.310	<0.001	<0.009	<0.001	<0.001	15.98	99.81	1.39	0.00	0.906
KC87-104E	38.01	0.006	0.13	0.332	10.89	0.091	41.77	0.374	<0.001	<0.009	0.004	<0.001	8.23	99.84	1.42	0.00	0.884
KC91-21A	39.08	0.051	0.93	0.370	13.78	0.204	43.10	0.366	0.42	<0.009	0.068	<0.001	1.88	100.25	1.42	0.03	0.861
KC91-21B	40.18	0.027	0.53	0.344	11.67	0.174	46.77	0.412	0.06	<0.009	0.336	<0.001	0.12	100.62	1.50	0.01	0.888
KC91-52A	38.17	0.033	0.57	0.127	11.47	0.025	37.29	0.337	0.68	<0.009	<0.001	<0.001	11.10	99.80	1.26	0.02	0.866
KC91-52B	37.96	0.035	0.52	0.398	11.56	0.177	45.76	0.386	0.12	<0.009	<0.001	<0.001	3.30	100.22	1.56	0.02	0.887
KC91-52D	40.08	0.023	0.34	0.338	8.18	0.131	48.64	0.420	0.12	<0.009	<0.001	<0.001	2.09	100.36	1.57	0.01	0.922
KC87-114G	40.03	0.062	1.22	0.167	7.75	0.087	40.34	0.312	<0.001	<0.009	<0.001	<0.001	10.20	100.17	1.30	0.03	0.912
KC87-114I	41.01	0.089	1.79	0.226	7.39	0.111	41.27	0.330	1.95	0.004	0.021	<0.001	5.96	100.15	1.30	0.05	0.917
KC87-114K	41.81	0.261	2.75	0.145	8.40	0.133	41.97	0.351	2.56	0.101	0.077	0.027	1.41	100.00	1.30	0.07	0.908
KC87-119A	42.49	0.155	3.99	0.399	10.60	0.180	35.21	0.259	4.32	0.252	0.031	0.008	1.62	99.51	1.07	0.11	0.868
KC87-102	39.35	0.187	4.07	0.497	10.87	0.128	32.81	0.202	1.91	0.205	0.055	0.005	9.27	99.56	1.08	0.12	0.857
KC91-52C	43.08	0.301	5.10	0.301	11.00	0.114	27.40	0.180	5.80	0.529	0.136	0.016	5.40	99.36	0.82	0.13	0.831
KC87-106A	51.50	0.155	5.32	0.258	7.91	0.267	21.38	0.131	9.55	0.507	0.700	0.007	1.35	99.04	0.54	0.12	0.843
Cape Uivak layered body																	
KC91-32A	39.96	0.046	1.25	1.145	10.08	0.192	43.99	0.363	0.48	<0.009	0.003	<0.001	2.45	99.96	1.42	0.04	0.896
KC91-32B	36.07	0.045	1.11	2.205	14.45	0.293	42.07	0.249	0.23	<0.009	<0.001	<0.001	3.07	99.79	1.50	0.03	0.852
KC91-32D	39.53	0.061	1.41	1.101	8.92	0.198	43.85	0.332	0.82	<0.009	<0.001	<0.001	3.86	100.08	1.43	0.04	0.907
KC91-32E	37.35	0.022	0.74	0.517	13.74	0.140	40.45	0.306	0.26	<0.009	<0.001	<0.001	6.65	100.18	1.40	0.02	0.854
KC91-32F	40.11	0.064	1.32	0.752	9.18	0.143	43.39	0.282	1.38	<0.009	<0.001	0.001	3.21	99.83	1.40	0.04	0.904
KC91-32C-1	41.39	0.711	3.95	0.885	15.83	0.164	25.43	0.172	7.36	0.068	0.021	0.027	3.02	99.03	0.79	0.11	0.761
KC91-32C-2	44.28	0.260	8.62	0.061	4.65	0.077	29.21	0.080	7.78	0.140	0.040	0.096	4.04	99.33	0.85	0.22	0.926
KC91-32C-3	43.38	0.674	4.73	0.591	12.25	0.149	26.66	0.141	7.90	0.113	0.031	0.036	2.65	99.31	0.79	0.12	0.812
KC91-32C-4	42.60	0.215	8.25	0.021	4.43	0.082	33.14	0.084	5.99	0.093	0.032	0.133	4.45	99.52	1.00	0.22	0.937
Metakomatiite suite																	
KC87-111E	50.35	0.143	5.62	0.500	10.29	0.239	27.51	0.259	3.56	0.549	0.127	<0.001	0.59	99.74	0.70	0.13	0.841
KC87-111F	44.32	0.240	8.47	0.582	13.63	0.155	26.81	0.187	3.95	0.531	0.080	0.024	0.97	99.95	0.78	0.22	0.796
KC87-111G	43.25	0.167	4.19	0.351	10.00	0.176	34.46	0.264	2.99	0.232	0.050	<0.001	3.53	99.66	1.03	0.11	0.872
KC87-111I	35.80	0.330	8.88	0.524	14.36	0.116	27.80	0.198	3.51	0.204	0.053	0.009	7.77	99.55	1.00	0.28	0.793
KC87-111K	45.57	0.233	6.58	0.456	9.86	0.134	25.44	0.196	8.62	0.804	0.160	<0.001	1.20	99.25	0.72	0.16	0.836
KC87-115D	49.16	0.437	5.05	0.309	13.84	0.270	19.23	0.125	10.05	0.762	0.179	0.028	0.12	99.56	0.50	0.12	0.734
Reference materials																	
MRG-1	39.16	3.84	8.46	0.069	18.07	0.172	13.46	0.020	14.95	0.72	0.20	0.055		99.18			
MRG-1 RV	39.12	3.77	8.47	0.063	17.94	0.170	13.55	0.025	14.70	0.74	0.18	0.080		98.81			
JP-1	43.19	0.007	0.67	0.432	8.50	0.122	45.48	0.324	0.55	<0.009	0.042	<0.001		99.32			
JP-1 RV	42.38	0.006	0.66	0.410	8.37	0.121	44.60	0.313	0.55	0.021	0.003	0.002		97.44			

Concentration values presented are in wt.%. LOl, loss on ignition. RV. Reference values of MRG-1 and JP-1 are from Govindaraju (1994) and Imai et al. (1995),

Table3

Table 3: Whole rock trace element compositions of selected Saglek ultramafic rocks from Northern Labrador, North Atlantic Craton

	Lithospheric mantle suite										*Metakomatiite suite*			*Reference materials*					
Rock type	Dunite			Amph harzburgite			Ol hornblendite			Hornblendite	Px hornblendite	Ol-Px hornblendite	Ol hornblendite	BIR-1 (n=3)		BCR-1 (n=2)		AGV-2 (n=4)		DTS-1 (n=4)	
Sample	KC87-104D	KC91-52B	KC91-52D	KC87-114K	KC91-32A	KC91-32E	KC91-52C	KC87-114G	KC87-114I	KC87-106A	KC87-111E	KC87-111G	KC87-111K	Avg.	RV	Avg.	RV, IV	Avg.	RV	Avg.	RV, IV
Ti*	0.0024	0.0214	0.0139	0.0796	0.0298	0.0119	0.1780	0.0375	0.0654	0.0956	0.0777	0.0967	0.1456	0.5777	0.5748	1.3115	1.3441	0.6138	0.6301	0.0026	0.0022
V	6.10	####	####	####	####	####	###	####	####	####	###	####	###	###	###	###	###	###	###	####	####
Cr*	0.1408	0.2647	0.2304	0.1072	0.7808	0.3589	0.1947	0.1163	0.1678	0.1684	0.2377	0.2345	0.3099	0.0384	0.0393	0.0016	0.0014	0.0016	0.0016	0.6463	0.4100
Co	####	###	###	###	###	###	####	####	####	####	####	###	####	####	####	####	####	####	####	###	###
Ni*	0.2093	0.2509	0.2690	0.2317	0.2420	0.2073	0.1228	0.1846	0.2250	0.0870	0.2531	0.1751	0.1323	0.0183	0.0169	0.0013	0.0012	0.0018	0.0019	0.3034	0.2298
Cu	0.266	0.590	1.72	1.09	0.628	0.318	####	0.774	1.39	8.19	###	3.11	9.42	###	###	####	####	####	####	2.37	5.70
Zn	####	####	####	####	###	####	####	####	####	####	####	####	####	####	####	###	###	###	####	####	####
Ga	0.592	1.06	0.797	2.88	1.92	1.18	6.52	1.57	1.99	7.92	6.51	4.63	7.04	####	####	####	####	####	####	0.572	*0.411*
Rb	0.289	0.017	0.629	1.18	1.37	0.0718	6.76	0.0190	0.434	####	1.46	1.05	1.10	0.178	0.210	####	####	####	####	0.0225	0.0660
Sr	0.410	0.264	1.04	9.37	1.82	1.13	####	2.54	7.90	6.64	####	5.80	####	###	###	###	###	###	###	0.578	0.300
Y	0.585	0.455	0.311	1.93	1.83	0.682	7.47	1.58	3.23	8.76	5.91	4.77	5.78	####	####	####	####	####	####	0.0373	0.0363
Zr	0.140	1.77	0.747	9.47	0.999	1.41	####	2.93	4.70	####	5.44	6.58	8.23	####	####	###	###	###	###	0.256	0.153
Nb	0.107	0.0881	0.0462	0.259	0.108	0.0505	0.585	0.100	0.234	0.457	0.203	0.178	0.196	0.491	0.553	####	####	####	####	0.0202	0.0154
Sn	0.170			0.103	0.0073	0.0158	0.326	0.0801	0.0941	1.06	0.236	0.0501	0.183	0.653	0.701	2.03	*2.44*	1.83	1.83	0.568	*0.600*
Sb	0.309	0.0066	0.0108	0.0013	0.0099	0.0098	0.0445	0.0014		0.0015	0.0021	0.0005	0.0013	0.576	0.462	0.353	0.632	0.586	0.458	0.814	0.473
Cs	0.0431	0.0073	0.101	0.0955	0.119	0.0239	2.70	0.0021	0.0191	1.90	0.0652	0.0654	0.0305	0.0046	0.0065	1.19	0.964	1.23	1.17	0.0007	0.0060
Ba	0.168	0.0626	0.423	2.51	1.13	0.410	5.15	0.391	2.68	####	0.785	1.00	2.87	6.01	6.75	###	###	####	####	####	0.342
La	0.0793	0.0711	0.0772	0.697	0.404	0.263	1.22	0.385	0.756	3.09	0.495	0.220	0.449	0.561	0.627	####	####	####	####	0.0203	0.0264
Ce	0.283	0.171	0.182	1.45	0.992	0.531	2.50	0.858	1.57	9.74	1.00	0.520	0.978	1.60	1.92	####	####	####	####	0.0350	0.0503
Pr	0.0595	0.0260	0.0304	0.229	0.165	0.0782	0.405	0.133	0.240	1.56	0.157	0.0972	0.164	0.353	0.372	6.67	6.77	8.40	8.17	0.0045	0.0061
Nd	0.301	0.133	0.129	1.00	0.784	0.345	2.11	0.622	1.13	6.15	0.795	0.614	0.880	2.37	2.40	####	####	####	####	0.0161	0.0232
Sm	0.108	0.0402	0.0342	0.258	0.215	0.088	0.749	0.186	0.338	1.36	0.296	0.307	0.408	1.08	1.11	6.40	6.60	5.56	5.51	0.0029	0.0044
Eu	0.0047	0.0018	0.0026	0.0733	0.0560	0.0219	0.150	0.0217	0.0496	0.370	0.0779	0.135	0.266	0.515	0.520	2.09	1.96	1.89	1.55	0.0051	0.0011
Gd	0.0870	0.0404	0.0379	0.272	0.219	0.095	0.734	0.185	0.348	1.63	0.336	0.288	0.410	1.03	1.81	7.46	6.73	7.60	4.68	0.0050	0.0041
Tb	0.0162	0.0083	0.0069	0.0460	0.0410	0.0162	0.165	0.0349	0.0657	0.226	0.0903	0.0833	0.107	0.278	0.362	1.02	1.06	0.767	0.651	0.0006	0.0007
Dy	0.101	0.0731	0.0536	0.348	0.306	0.119	1.33	0.274	0.525	1.49	0.870	0.770	0.993	2.56	2.54	6.27	6.39	3.52	3.55	0.0043	0.0050
Ho	0.0186	0.0169	0.0115	0.0723	0.0693	0.0249	0.285	0.0575	0.116	0.323	0.209	0.177	0.218	0.569	0.572	1.27	1.27	0.670	0.682	0.0011	0.0014
Er	0.0504	0.0516	0.0394	0.215	0.213	0.0803	0.833	0.169	0.350	0.959	0.673	0.544	0.666	1.72	1.68	3.59	3.66	1.84	1.83	0.0046	0.0049
Tm	0.0082	0.0076	0.0067	0.0319	0.0340	0.0121	0.119	0.0221	0.0528	0.141	0.107	0.0793	0.0987	0.250	0.256	0.506	0.535	0.256	0.262	0.0010	0.0010
Yb	0.0613	0.0478	0.0494	0.198	0.222	0.0848	0.741	0.127	0.336	0.917	0.699	0.510	0.633	1.59	1.63	3.20	3.38	1.58	1.65	0.0101	0.0095
Lu	0.0107	0.0087	0.0087	0.0304	0.0361	0.0140	0.106	0.0154	0.0523	0.140	0.110	0.0755	0.0952	0.232	0.248	0.469	0.499	0.240	0.251	0.0019	0.0021
Hf	0.0100	0.0478	0.0220	0.247	0.0535	0.0479	0.505	0.093	0.122	0.349	0.173	0.217	0.249	0.580	0.582	4.70	4.92	5.15	5.14	0.0066	0.0053
Ta	0.0497	0.0056	0.0035	0.0144	0.0065	0.0023	0.0407	0.0081	0.0149	0.0234	0.0096	0.0073	0.0080	0.0413	0.0414	0.747	0.786	0.832	0.865	0.0005	0.0012
W	0.200	0.130	0.201	1.75	0.280	0.235	0.298	0.0530	0.0880	0.101	0.0690	0.0480	0.0340								
Pb	0.583	0.437	0.481	1.68	0.393	0.369	2.53	0.701	0.582	4.30	1.35	0.849	3.16	3.08	3.04	####	####	####	####	4.24	8.50
Th	0.0248	0.0268	0.0213	0.126	0.0670	0.0409	0.170	0.0438	0.0681	0.131	0.137	0.123	0.0390	0.0227	0.0328	6.04	5.79	6.57	6.17	0.0053	0.0098
U	0.0201	0.0067	0.0167	0.116	0.0391	0.0236	0.299	0.0296	0.0239	0.156	0.150	0.0523	0.0884	0.0103	0.0105	1.62	1.68	1.87	1.89	0.0031	0.0032

Concentration values presented are in µg/g except for Ti, Cr and Ni in g/100 g. Concentration of W are from Liu et al. (2016). Reference values (RV) and information values (IV in italics) are from Jochum *et al.* (2016).

Table4

Table 4: HSE concentrations and Re-Os isotopes data of Saglek ultramafic rocks from Northern Labrador, North Atlantic Craton

Sample	Os (ng/g)	Ir (ng/g)	Ru (ng/g)	Pt (ng/g)	Pd (ng/g)	Re (ng/g)	$^{187}Re/^{188}Os$	$^{187}Os/^{188}Os$	T_{RD} (Ga)	T_{Ma} (Ga)	$^{187}Os/^{188}Os_i$ (Sm-Nd)	γOs_i
Lithospheric mantle suite												
KC87-104D	4.44	3.65	6.02	0.048	0.125	0.0078	0.0084 (8)	0.10557 (6)	3.15	3.21	0.10509	1.2
KC87-104E	4.36	3.83	6.25	0.205	0.109	0.0145	0.0160 (7)	0.10534 (5)	3.18	3.31	0.10442	0.5
KC91-21A	2.57	2.43	5.63	0.960	1.08	0.0471	0.0881 (26)	0.10544 (6)	3.17	4.01	0.10036	-3.4
KC91-21B	2.23	2.07	5.77	0.542	0.793	0.0236	0.0507 (9)	0.10412 (25)	3.35	3.81	0.10119	-2.6
dupl.	2.50	2.03	5.53	0.567	0.448	0.0175	0.0336 (22)	0.10453 (38)	3.29	3.58	0.10259	-1.2
KC91-52A	3.57	3.38	4.18	0.753	0.274	0.0042	0.0057 (5)	0.10786 (24)	2.83	2.87	0.10753	3.5
KC91-52B	3.86	3.04	6.23	0.583	0.180	0.0096	0.0120 (4)	0.10558 (17)	3.15	3.24	0.10488	1.0
dupl.	4.12	3.00		0.626	0.119	0.0083	0.010 (13)	0.10554 (14)	3.15	3.23	0.10499	1.1
KC91-52D	4.15	3.68	6.14	0.546	0.209	0.0060	0.0069 (2)	0.10529 (15)	3.19	3.24	0.10489	1.0
KC91-52C	1.09	1.31	5.66	7.82	6.77	0.556	2.49 (9)	0.21283 (37)		2.41		
dupl.	1.13	1.30	5.46	8.20	6.42	0.480	2.07 (4)	0.20934 (55)		2.88		
KC87-114G	4.08	3.83	3.05	0.849	0.558	0.0073	0.0086 (11)	0.10481 (29)	3.25	3.32	0.10431	0.4
KC87-114I	4.31	2.56	4.29	0.528	0.494	0.0056	0.0062 (7)	0.10458 (5)	3.29	3.34	0.10422	9.4
KC87-114K	7.03	4.57	4.02	10.5	4.17	0.0058	0.0040 (4)	0.10504 (3)	3.22	3.25	0.10481	10.0
dupl.	4.05	2.94	3.67	3.61	3.01	0.0049	0.0058 (8)	0.10626 (4)	3.05	3.10	0.10593	11.1
KC87-119A	2.56	1.84	5.43	6.47	7.85	0.384	0.724 (8)	0.14171 (7)		2.63	0.10002	4.9
dupl.1	2.46	1.81	4.97	7.78	7.25	0.375	0.735 (7)	0.14344 (5)		2.85	0.10109	6.1
dupl.2	2.97	1.97	5.07	7.02	7.13	0.377	0.613 (6)	0.13651 (3)		2.56	0.10117	6.2
dupl.3	2.66	1.97	5.14	7.16	7.22	0.374	0.679 (7)	0.14037 (4)		2.77	0.10126	6.2
dupl.4	2.54	1.82	5.44	5.86	7.94	0.427	0.811 (16)	0.14918 (49)		3.14	0.10245	7.5
KC87-119A2	2.55	1.98	5.77	6.19	6.15	0.418	0.794 (58)	0.17177 (9)			0.12602	32.2
KC87-102	0.867	0.78	6.38	3.33	3.95	0.0061	0.0339 (31)	0.10581 (18)	3.12	3.39	0.10386	9.0
dupl.		0.88	6.21	3.87	3.86	0.0049						
KC87-106A	1.10	0.815	2.55	10.3	11.8	0.159	0.702 (18)	0.13875 (18)		2.30		
Cape Uivak layered body												
KC91-32A	0.923	0.938	10.1	1.78	0.938	0.0020	0.0106 ####	0.10689 (61)	2.97	3.04	0.10628	11.5
KC91-32B	4.09	2.13	16.2	33.0	0.780	0.0142	0.0167 (16)	0.10578 (13)	3.12	3.25	0.10481	10.0
KC91-32D	0.839	0.583	11.0	1.20	0.925	0.0063	0.0358 (65)	0.10603 (59)	3.09	3.37	0.10397	9.1
KC91-32E	3.22	2.83	8.14	0.925	0.599	0.0194	0.0290 (22)	0.10512 (29)	3.21	3.45	0.10345	8.5
KC91-32F	0.654	0.512	8.27	1.90	1.02	0.0033	0.0246 (66)	0.10591 (20)	3.10	3.29	0.10450	9.6
KC91-32C-1	1.55	1.30	10.4	15.0	8.20	0.0056	0.0175 (34)	0.10577 (6)	3.12	3.26	0.10476	9.9
KC91-32C-2	0.052	0.025	0.246	1.56	5.29	0.0052	0.483 (70)	0.1182 (11)	1.37			
KC91-32C-3	1.22	0.811	6.22	13.8	11.3	0.0057	0.0223 (63)	0.10658 (40)	3.01	3.18	0.10530	10.5
KC91-32C-4	0.031	0.006	0.084	0.812	2.76	0.0106	1.63 (34)	0.1504 (66)		1.11		
Metakomatiite suite												
KC87-111E	2.41	2.45	4.00	6.90	16.9	0.533	1.07 (5)	0.16766 (42)		3.54	0.09815	11.3
dupl.	2.45	1.93	4.13	6.90	16.1	0.556	1.10 (5)	0.17085 (48)		3.63	0.09915	12.6
KC87-111F	2.82	2.32	5.27	12.1		0.0795	0.136 (3)	0.14281 (42)			0.13396	
dupl.	2.82	2.18	5.56	14.3	61.1	0.0750	0.129 (5)	0.1678 (59)			0.15945	
KC87-111G	2.78	2.05	4.35	2.21	5.37	0.0062	0.0106 (9)	0.10284 (2)	3.53	3.62	0.10214	7.3
dupl.	3.45	2.43	4.43	2.55	7.05	0.0068	0.0094 (5)	0.10245 (1)	3.58	3.66	0.10184	6.9
KC87-111I	3.91	2.33	7.63	9.67	2.52	0.0117	0.0143 (7)	0.10278 (2)	3.54	3.66	0.10185	7.0
dupl.1	3.20	2.44	7.03	9.52	2.12	0.0095	0.0143 (6)	0.10281 (5)	3.53	3.65	0.10188	7.0
dupl.2	2.24	2.12	7.00	9.91	2.48	0.0097	0.0209 (8)	0.10370 (1)	3.41	3.59	0.10234	7.5
KC87-111K	1.72	1.43	4.86	12.1	24.0	0.0024	0.0068 (14)	0.10230 (12)	3.60	3.66	0.10185	6.9
dupl.	1.63	1.28	4.61	11.2	21.5	0.0025	0.0074 (8)	0.10233 (4)	3.60	3.66	0.10185	6.9
KC87-115D	0.397	0.444	1.48	2.69	3.58	0.444	5.58 (19)	0.3992 (4)		3.07		
Reference materials												
UB-N (n=13)	3.85	3.41	6.80	6.93	5.59	0.207	0.263	0.12728				
1SD	0.39	0.26	0.47	0.16	0.17	0.015	0.035	0.00074				
JP-1 (n=15)	3.10	2.78	5.59	4.57	1.45	0.0241	0.0387	0.12083				
1SD	0.57	0.34	0.75	0.91	0.22	0.0018	0.0090	0.00070				

Analyses recalculated on an anhydrous basis; dupl., duplicate analyses; $^{187}Os/^{188}Os$ ratios normalised using $^{192}Os/^{188}Os = 3.08271$ and corrected using $^{18}O/^{16}O$ and $^{17}O/^{16}O$ of 0.002045 and 0.000371 respectively; Uncertainties on $^{187}Re/^{188}Os$ and $^{187}Os/^{188}Os$ (given in brackets, refer to least significant digits) are estimated by error propagation of isotope measurements (2SE) and blank correction. T_{RD} and T_{MA} ages (Ga) are calculated by using ^{187}Re decay constant $\lambda_{Re} = 1.666 \times 10^{-11}$ year^{-1} relative to the evolution of average chondrite with initial $^{187}Os/^{188}Os = 0.09531$ at 4.558 Ga, and $^{187}Re/^{188}Os = 0.40186$ (Smoliar et al., 1996; Shirey and Walker, 1998). Initial $^{187}Os/^{188}Os$ ratios are recalculated by using age values of Sm-Nd isochrons, which are 3.362 Ga for lithospheric mantle suite including Cape Uivak layered body, and 3.782 Ga for metakomatiite suite, respectively (Morino et al., 2017). Gamma Os values refer to the percent deviation relative to the average chodrite at the time of emplacement. Unrealistic values of model ages, initial $^{187}Os/^{188}Os$ ratios and gamma Os values are not presented. Full data and compilation of published values for UB-N and JP-1 are in Ishikawa *et al.* (2014).